

spin-diffusion becomes meaningless as each pair of protons may exhibit either behavior or behavior between the extremes. The relative sign of a cross-peak will not necessarily accurately reflect the rate of global molecular reorientation. Extreme-narrowing (anti-phase with respect to the diagonal) cross-peaks observed in NOESY spectra of macromolecules should not be ignored or automatically assigned to artifacts. The simulations show that motional averaging about an angle in the range of 50° to 60° will produce this type of cross-peak. Indeed, confirmation of a negative cross-peak would yield a new structural constraint. A spatial constraint would define a range of angles for the orientation of motional averaging of a proton pair with respect to the major axis of global molecular reorientation.

The calculations indicate that highly anisotropic molecular orientation will produce results that cannot be explained by calculations on the basis of the rigid isotropic assumptions. Oriented molecules in lipid bilayers and micelles or semiflexible polymers encountered in material sciences demand application

of the full spectral density functions. In extremely high magnetic fields (¹H frequencies >500 MHz) molecules with large dipole moments are known to align along the direction of the static field. The results for highly anisotropic motion ($\tau_1 \ll \tau_2$) would become important under these circumstances.

While we have only considered isolated spin pairs, the spatial aspects of spin topology and internal motion will be important for understanding cross-relaxation in multiple-spin relaxation networks. Multiple-spin networks, including the effects cross-correlated spectral densities, are now under investigation in our laboratories.

Supplementary Material Available: An Appendix describing the theoretical section in more detail, additional plots of the angular dependence of η , the NOESY cross-peak evolution for a variety of molecular sizes and shapes, and tables containing calculations of η and distance errors for oblate ellipsoids (47 pages). Ordering information is given on any current masthead page.

Tl^I–Tl^I and In^I–In^I Interactions: From the Molecular to the Solid State

Christoph Janiak and Roald Hoffmann*

Contribution from the Department of Chemistry and Materials Science Center, Cornell University, Ithaca, New York 14853. Received November 6, 1989

Abstract: The influence of the ligand geometry on Tl^I–Tl^I and In^I–In^I bonding has been studied within the extended Hückel framework, looking at the following observed molecular and solid-state structures or structural types (respective metal moiety given in parentheses): {(PhCH₂)₅C₅Tl/In}₂ (dimer), {TlOMe}₄ (bridged tetramer), Tl₂Te₂²⁻ (bridged dimer), {Me₅C₅In}₆ (octahedral hexamer), {MeC₅H₄In}_∞ (dimers), TlS = Tl^ITl^{III}S₂ (TlSe-type, linear chains), In₁₁Mo₄₀O₆₂ (chain segments), InMo₄O₆ (linear chain), and TiCo₂S₂ (ThCr₂Si₂-type, square-planar nets). For Tl^I and In^I complexes with large Tl^I...Tl^I and In^I...In^I separations the ligand environment (especially the L–M–M angle) is found to be the dominant factor in determining the extent of the bonding interaction between the metals. The metal–metal distances in these compounds range from about 265 to 400 pm. We have interpreted the metal–metal interaction in these systems with the help of model complexes, such as Tl₂, Tl₂H₂, {C₅H₅Tl/In}₂, {TlOMe}₂, {HIn}₆, {C₅H₅In}₆, Tl/In_∞, {TiH₄/S₄}_∞, {InO₄}_∞, Tl_{inets}, and {TiH₄/S₄}_{inets} with the ligands in various geometrical arrangements. Starting the analysis with a bare Tl₂ dimer or Tl_∞ chain, it is shown that a mixing of empty p levels into the filled s combinations is the basis for a bonding interaction. The behavior of the overlap population as a function of the ligand geometry is then studied. A detailed angle variation in Tl₂H₂ helped us to understand why one passes from an almost nonbonding situation in the linear arrangement, over a region of strong bonding upon trans-bending of the hydrogens, to again reach a nonbonding interaction in the bridging geometry. What happens in the trans-bending in Tl₂H₂ is closely related to the orbital interactions in the pyramidalization of AH₃ systems (e.g. NH₃) and the bending of AH₂ molecules (e.g. H₂O). Calculations on the more realistic examples {TlOMe}₂, {C₅H₅Tl/In}₂, and Tl₂Te₂²⁻ confirmed that a trans-bent geometry with a ligand–M–M angle close to 120° gives an optimum overlap population at a relatively long, fixed Tl^I–Tl^I or In^I–In^I separation in molecular systems. A bridging ligand geometry, either in a molecular complex or in an extended structure, generally gave a non- or antibonding metal–metal overlap population. This is in agreement with the apparent general consensus in the literature that the bridged species do not display any Tl–Tl interactions. Dimers where the trans-bent geometry has been observed, despite their long M–M contacts (such as 363 pm as in {(PhCH₂)₅C₅Tl/In}₂), can be assigned a definite M^I–M^I bonding interaction. The bonding in solid-state structures with Tl^I–Tl^I or In^I–In^I contacts was analyzed with the help of band structure diagrams, density of state, and crystal orbital overlap population plots. A prior look at the interaction in a (molecular) Tl₂ dimer in a square-pyramidal or cubic ligand field facilitated the interpretation. Extended structures showed an optimum at ligand–M–M angles of 90°, resulting in a square-planar ligand field for metal chains or an on-top/bottom position in metal nets. While a square-planar ligand field increases the s–p_z mixing, hence overlap population, with respect to the bare Tl/In chain or net, a cubic ligand environment widens the s–p_z energy gap, thereby decreasing mixing and overlap population.

Introduction

With this paper we provide some material for a discussion of thallium(I)–thallium(I) and indium(I)–indium(I) interactions whose tendencies to form unusual contacts cannot be overlooked, yet whose bonding character remains mostly unclear. We will carry out our theoretical study on the basis of the very simple, semiempirical, extended Hückel formalism. We are aware of its limitations: It is a one-electron model with no spin–orbit coupling, no configuration interaction. Relativistic effects, likely to be

important for heavy atoms, are not accounted for explicitly, only in our choice of parameters (which may be problematic in itself). We also cannot satisfactorily optimize most structures. But we are certain that within our model we can develop a chemical understanding, an analysis of those structural types in which Tl^I–Tl^I and In^I–In^I bonding interactions are likely to be present.

Of course, the problems discussed here are related to the larger question of stereochemical activity of a lone pair in compounds of elements that have an s² configuration.¹

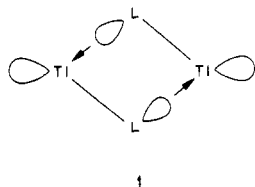
Table I. Tl...Tl Bridged Molecular Complexes^a

formula	d(Tl...Tl)/pm	ref
Tl(μ ³ -OCH ₃) ₄	384	5
TlTeI ₂ ²⁻	360.0 (3)	6
Tl ₆ [μ ³ -Fe(CO) ₃] ₄ [μ ² -Fe(CO) ₄] ₂ [Fe(CO) ₄] ₄ ⁶⁻	370.6 (1)-377.3 (1)	7
Tl(TolNNNNNTol) ₂	343.0 (1)	8
Tl(PhNNNPh) ₂	364.1 (1)	8
Tl ₂ [N ^t Bu] ₂ (N ^t Bu) ₂ (MeSi) ₂	365.3 (1)	9
Tl ₂ [μ ² -Fe(CO) ₄] ₂ [Fe(CO) ₄] ₂ ²⁻	365.8 (5)	10
Tl ₄ [μ ² -Fe(CO) ₄] ₂ [μ ² -Fe ₂ (CO) ₇] ₂ [Fe(CO) ₄] ₄ ⁴⁻	360.4 (3), 385.9 (2)	10
Tl ₂ [μ ² -Fe(CO) ₄] ₂ [Fe ₂ (μ-CO) ₂ (CO) ₆] ₂ ²⁻	350.7 (1)	11
Tl(μ ³ -OSiPh ₃) ₄	379.8 (2)-397.2 (3)	12
{Tl ₂ (OSiMe ₂) ₂ O} ₂ _n	379.8 (2)-433.3 (2)	12

^a Limit for Tl...Tl contacts reported here, arbitrarily set at 400 ppm; bridging atoms are underlined. Abbreviations: Tol = tolyl; Ph = phenyl; Me = methyl; ^tBu = *tert*-butyl.

Molecular Complexes

The formation and verification of a genuine molecular thallium-thallium bond is still an open problem in main group 13 chemistry. Apparently no Tl^I...Tl^I distances below 305 pm (with the exception of a recent Tl^{II}-Tl^{II} dimer in the solid, to be discussed below) and only one below 340 pm have been observed so far. These distances correspond to twice the value of the covalent radius (estimated at 152 pm from Tl(CH₃)₃)² or the separation found in thallium metal.³ But a number of molecular thallium complexes are reported in the literature that show Tl^I...Tl^I distances between 360 and 400 pm (400 pm being twice the van der Waals radii for Tl^I). The majority of these compounds exhibit the feature of the two thalliums being bridged by two or three ligands (1). The bridge formation can be interpreted as an attempt by



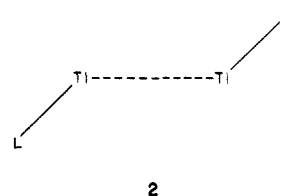
the coordinatively unsaturated metal to fill its coordination sphere by an available lone pair of a main group V or VI element or a metal carbonyl fragment (see Table I) in the ligand. Empty (p) orbitals on thallium(I) are available to receive that donation. A schematic bonding arrangement is shown in 1.

Table I (not meant to be a complete list) summarizes some of the examples. In the literature there is little cross-referencing or consistent interest in bridged thallium species. There was some discussion early on about the possibility of Tl...Tl interactions and bonding, and weak Tl...Tl interactions for the tetrameric thalli-

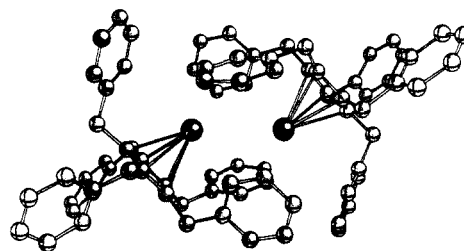
um(I) alkoxides were deduced from their Raman and infrared spectra.¹³ At this time, the consensus, such as it is, seems to be that none of the bridged species show any substantial metal...metal bonding interactions. Such short Tl...Tl contacts as may be found in bridged complexes have to be interpreted simply as resulting from the bridging configuration. This view is supported by an extended Hückel molecular orbital calculation on the Zintl metal carbonylate [Tl₆Fe₁₀(CO)₃₆]⁶⁻, where a small Tl...Tl overlap population of 0.025 was found and was interpreted as a nonbonded contact.⁷ So far, this example seems also to be the only one that has been studied theoretically. We do find some theoretical studies on the bare Tl₂⁰ or Tl₂¹⁺ species. Both are not only experimentally known diatomics,¹⁴⁻¹⁶ but there is also great theoretical interest in them, stemming from efforts to gauge relativistic effects on the bonding between two heavy atoms.¹⁷⁻²³

We would like to point out that a chemist might intuitively, i.e. based on VSEPR²⁴ arguments, place the lone pair electrons on thallium in 1—if he assigns them any directionality—outside of the ring or cage formed by the thalliums and bridging ligands, as depicted in 1. This leaves no substantial electron density along the Tl-Tl axis.

However, there exist a few recent examples where the Tl...Tl moiety is not bridged by its ligands. Rather, the ligands are arranged in a trans-bent geometry, as shown in 2. One such



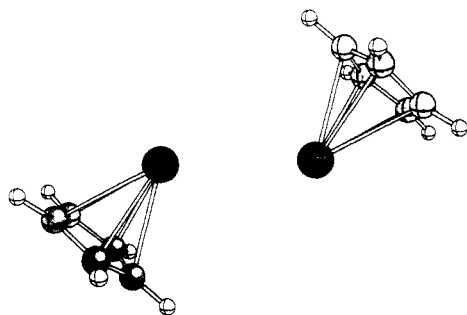
molecule is a modification of pentabenzylcyclopentadienyl-thallium,²⁵ [(PhCH₂)₅C₅Tl]₂ (3, 4). Synthesized by Schumann and co-workers, it has a ligand-Tl-Tl angle of 131.8°. 3 shows the full structure and 4 the "core" unit, with the benzyl groups replaced by hydrogen for clarity. The absence of lone-pair



electrons on the (PhCH₂)₅C₅ ligand makes, of course, a bridging geometry unlikely. Aside from being a centrosymmetric dimer,

- (1) (a) Ng, S.-W.; Zuckerman, J. J. *Adv. Inorg. Chem. Radiochem.* **1985**, *29*, 297. (b) Donaldson, J. D.; Grimes, S. R. *Rev. Silicon, Germanium, Tin, Lead Compd.* **1984**, *8*, 1. (c) Galy, J.; Meunier, G.; Anderson, S.; Aström, A. *J. Solid State Chem.* **1975**, *13*, 142. (d) Brown, I. D. *Ibid.* **1974**, *11*, 214. (e) Gillespie, R. J. *J. Chem. Educ.* **1970**, *47*, 18. (f) Dunitz, J. D.; Orgel, L. E. *Adv. Inorg. Chem. Radiochem.* **1960**, *2*, 19.
- (2) Sheldrick, G. M.; Sheldrick, W. S. *J. Chem. Soc. A* **1970**, 28.
- (3) (a) Wyckoff, R. W. G. In *Crystal Structures*, 2nd ed.; Interscience Publishers: New York, 1963; Vol. 1. (b) Wells, A. F. In *Structural Inorganic Chemistry*, 4th ed.; Oxford University Press: London, 1975; p 1013.
- (4) Huheey, J. E. In *Inorganic Chemistry*, 3rd ed.; Harper and Row: New York, 1983; p 259.
- (5) Dahl, L. F.; Davis, G. L.; Wampler, D. L.; West, R. *J. Inorg. Nucl. Chem.* **1962**, *24*, 357.
- (6) Burns, R. C.; Corbett, J. D. *J. Am. Chem. Soc.* **1981**, *103*, 2627.
- (7) Whitmire, K. H.; Ryan, R. R.; Wasserman, H. J.; Albright, T. A.; Kang, S.-K. *J. Am. Chem. Soc.* **1986**, *108*, 6831.
- (8) Beck, J.; Strähle, J. Z. *Naturforsch.* **1986**, *41b*, 1381.
- (9) Veith, M.; Goffing, F.; Huch, V. *Chem. Ber.* **1988**, *121*, 943.
- (10) Whitmire, K. H.; Cassidy, J. M.; Rheingold, A. L.; Ryan, R. R. *Inorg. Chem.* **1988**, *27*, 1347.
- (11) Cassidy, J. M.; Whitmire, K. H. *Inorg. Chem.* **1989**, *28*, 1432.
- (12) Harvey, S.; Lappert, M. F.; Raston, C. L.; Skelton, B. W.; Srivastava, G.; White, A. H. *J. Chem. Soc., Chem. Commun.* **1988**, 1216.

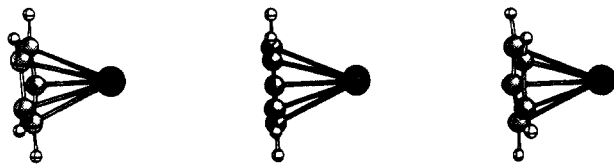
- (13) Maroni, V. A.; Spiro, T. G. *Inorg. Chem.* **1968**, *7*, 193. See also: Burke, P. J.; Matthews, R. W.; Gillies, D. G. *J. Chem. Soc. Dalton* **1980**, 1439.
- (14) Huber, K. P.; Herzberg, G. In *Molecular Spectra and Molecular Structure IV. Constants of Diatomic Molecules*; van Nostrand Reinhold: New York, 1979; p 648ff.
- (15) Berkowitz, J.; Walter, T. A. *J. Chem. Phys.* **1968**, *49*, 1184.
- (16) Balducci, G.; Piacente, V. *J. Chem. Soc., Chem. Commun.* **1980**, 1287.
- (17) (a) Pitzer, K. S. *Acc. Chem. Res.* **1979**, *12*, 271. (b) Pitzer, K. S. *Int. J. Quantum Chem.* **1984**, *25*, 131.
- (18) Christiansen, P. A.; Pitzer, K. S. *J. Chem. Phys.* **1981**, *74*, 1162.
- (19) Hafner, P.; Habitz, P.; Ishikawa, Y.; Wechsel-Trakowski, E.; Schwarz, W. H. E. *Chem. Phys. Lett.* **1981**, *80*, 311.
- (20) Christiansen, P. A. *J. Chem. Phys.* **1983**, *79*, 2928.
- (21) Pyykkö, P. *Chem. Rev.* **1988**, *88*, 563.
- (22) Ermler, W. C.; Ross, R. B.; Christiansen, P. A. *Adv. Quant. Chem.* **1988**, *19*, 139.
- (23) Balasubramanian, K. *Chem. Rev.* **1990**, *90*, 93.
- (24) Gillespie, R. J. In *Molecular Geometry*; Van Nostrand Reinhold: New York, 1972.
- (25) Schumann, H.; Janiak, C.; Pickardt, J.; Börner, U. *Angew. Chem.* **1987**, *99*, 788; *Angew. Chem., Int. Ed. Engl.* **1987**, *26*, 789.



4

3 also features a presumably mainly covalent thallium–cyclopentadienyl interaction, while the parent cyclopentadienyl²⁶ or even pentamethylcyclopentadienylthallium²⁷ adopt ionic, polymeric structures of zig-zag chains in the solid state. Yet, the Tl...Tl distance of 363.2 pm in **3** is like those found in bridged species. To us a Tl...Tl contact only about 20 pm longer than in Tl metal, occurring in the absence of bridging, is definitely suggestive of direct metal–metal bonding.

From the nature of the bulky ligand in **3** it might seem more appropriate to discuss the formation of the “dimeric” pentabenzylcyclopentadienylthallium unit in terms of an organic envelope interaction (cf. geared stacking of benzene in its crystal structure²⁸). However, the discovery of a second crystalline modification of (PhCH₂)₅C₅Tl, where the monomeric, covalent species are arranged in a linear chain²⁹ (**5**, benzyl groups replaced by hydrogen for clarity), makes the dimer more intriguing. Fast crystallization yields the linear allotrope, whereas upon slow crystallization the dimer is obtained, being apparently the thermodynamically more stable allotrope.



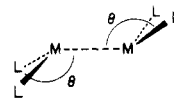
5

In both cases (**3** and **5**) it is probably correct to attribute the packing in a first approximation to the ligand–ligand interactions that create the “big hole” on the potential surface. However, Tl–Tl interactions may become important in **3**, shaping the bottom of that potential energy well.

Other examples with unbridged Tl...Tl moieties include a 1,3,5-tri-*tert*-butyl-6-methyl-1,3,5-triazonia-6-sila-2,4,7-trithalliatricyclo[3.1.1.0^{3,6}]heptane dimer, [MeSi(N^{*t*}Bu)₃Tl₃]₂, with one remarkable short Tl¹–Tl¹ contact of 315 to 318 pm and ten other Tl¹...Tl¹ separations between 346 and 393 pm (synthesized by Veith and co-workers).^{30,31} Jutzi and coworkers also have provided some relevant structures, a Tl–carbolide and a Tl–fulvene with intermolecular Tl¹...Tl¹ contacts of 360 to 370 pm in an extended array.³²

With the impetus of the dimeric (PhCH₂)₅C₅Tl structure, we were encouraged to examine the question of Tl¹–Tl¹ bonding interactions in molecular and extended compounds and to extend it to In^I compounds. These are the subjects of this paper.

The structure of **3** and part of its properties are reminiscent of the divalent group IV alkyls {[(Me₃Si)₂CH]₂M₂} (M = Ge, Sn) (**6**), synthesized and studied in detail by Lappert and co-workers.³³ Although the metal–metal distance in bis[bis(trimethylsilyl)methyl]germylene^{33a} and -stannylene^{33a,b} (234.7 and 276.4 pm)



6

is much shorter—not just in comparison to the thallium complex, but also to M–M distances in germanium or tin metal (245 and 302 pm)—some of the properties of all three complexes are strikingly similar: All three are dimeric *only* in the solid state, and monomeric in solution and in the gas phase.^{33–36} Also, the ligand–M–ligand plane forms an angle θ of 148° (Ge) or 138° (Sn) with the M–M axis (see **6**). The bonding in the parent digermylene, H₂Ge–Ge₂, and distannylene, H₂Sn–SnH₂, has been studied in quite some detail.^{34–39} If the bulky alkyls in **6** are replaced by suitable lone pair containing chalcogenide or amide ligands (with not too bulky substituents on the α -O or -N atom), bridging structures similar to **1** are encountered as well.^{31,40} We will return below to differences and similarities in the MO diagrams between H₂Ge–GeH₂ and our model system HTl–TlH.

Indium(I) compounds are less abundant than those of its heavier homologue thallium(I), primarily due to the fact that +III is the preferred oxidation state for indium, and its +I state is less accessible and more unstable than the +I state for thallium. That makes the existing indium(I) compounds even more interesting. Apparently, there are known to date only two molecular In^I complexes that feature In...In contacts below 400 pm: an octahedral “hexameric cluster” of pentamethylcyclopentadienylindium(I) (Beachley, Jr., and co-workers)⁴¹ (7, In...In = 394.2 to 396.1 pm, only the centroid of each pentamethylcyclopentadienyl group shown as a light grey ball, for clarity) and the indium derivative of pentabenzylcyclopentadienyl (Schumann and co-workers)⁴² being isostructural to **3** with In...In = 363.1 pm. Normal cyclopentadienyl or methylcyclopentadienylindium show again an ionic, polymeric, zig-zag chain structure in the solid.^{26,43} At first sight, having the same metal–metal distance in both the indium and the thallium derivative of (PhCH₂)₅C₅ seems to support the notion that a packing effect of the ligand enforces dimerization of these molecules by van der Waals fitting of the organic envelope, rather than as a consequence of metal–metal interaction. However, one could also argue that interaction of

(33) (a) Goldberg, D. E.; Harris, D. H.; Lappert, M. F.; Thomas, K. M. *J. Chem. Soc., Chem. Commun.* **1976**, 261. (b) Davidson, P. J.; Harris, D. H.; Lappert, M. F. *J. Chem. Soc. Dalton* **1976**, 2268. (c) Cotton, J. D.; Davidson, P. J.; Lappert, M. F. *Ibid.* **1976**, 2275. (d) Cotton, J. D.; Davidson, P. J.; Lappert, M. F.; Donaldson, J. D.; Silver, J. *Ibid.* **1976**, 2286. (e) Hitchcock, P. B.; Lappert, M. F.; Miles, S. J.; Thorne, A. J. *J. Chem. Soc., Chem. Commun.* **1984**, 480.

(34) Fjeldberg, T.; Haaland, A.; Lappert, M. F.; Schilling, B. E. R.; Seip, R.; Thorne, A. J. *J. Chem. Soc., Chem. Commun.* **1982**, 1407.

(35) Fjeldberg, T.; Haaland, A.; Schilling, B. E. R.; Volden, H. V.; Lappert, M. F.; Thorne, A. J. *J. Organomet. Chem.* **1985**, 280, C43.

(36) Fjeldberg, T.; Haaland, A.; Schilling, B. E. R.; Lappert, M. F.; Thorne, A. J. *J. Chem. Soc. Dalton* **1986**, 1551.

(37) Trinquier, G.; Malrieu, J.-P.; Rivière, P. *J. Am. Chem. Soc.* **1982**, 104, 4529.

(38) Nagase, S.; Kudo, T. *J. Mol. Struct. Theochem.* **1983**, 103, 35.

(39) Dewar, M. J. S.; Grady, G. L.; Kuhn, D. R.; Merz, K. M. *J. Am. Chem. Soc.* **1984**, 106, 6773.

(40) (a) Hitchcock, P. B.; Lappert, M. F.; Samways, B. J.; Weinberg, E. L. *J. Chem. Soc., Chem. Commun.* **1983**, 1492. (b) Fjeldberg, T.; Hitchcock, P. B.; Lappert, M. F.; Smith, S. J.; Thorne, A. J. *J. Chem. Soc., Chem. Commun.* **1985**, 939. (c) Veith, M. *Angew. Chem.* **1987**, 99, 1; *Angew. Chem., Int. Ed. Engl.* **1987**, 26, 1.

(41) (a) Beachley, O. T., Jr.; Blom, R.; Churchill, M. R.; Faegri, K., Jr.; Fettinger, J. C.; Pazik, J. C.; Victoriano, L. *Organometallics* **1989**, 8, 346. (b) Beachley, O. T., Jr.; Churchill, M. R.; Fettinger, J. C.; Pazik, J. C.; Victoriano, L. *J. Am. Chem. Soc.* **1986**, 108, 4666.

(42) Schumann, H.; Janiak, C.; Görlitz, F.; Loebel, J.; Dietrich, A. *J. Organomet. Chem.* **1989**, 363, 243.

(43) Beachley, O. T., Jr.; Pazik, J. C.; Glassman, T. E.; Churchill, M. R.; Fettinger, J. C.; Blom, R. *Organometallics* **1988**, 7, 1051.

(26) Frasson, E.; Menegus, F.; Panattoni, C. *Nature London* **1963**, 199, 1087.

(27) Werner, H.; Otto, H.; Kraus, H. J. *J. Organomet. Chem.* **1986**, 315, C57.

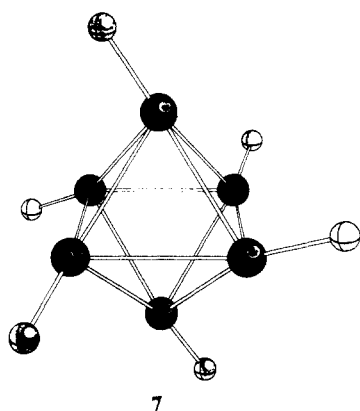
(28) (a) Cox, E. G.; Cruickshank, D. W. J.; Smith, J. A. S. *Proc. R. Soc. London Ser.* **1958**, A247, 1. (b) Piermarini, G. J.; Mighell, A. D.; Weir, C. E.; Block, S. *Science* **1969**, 165, 1250.

(29) Schumann, H.; Janiak, C.; Khan, M. A.; Zuckerman, J. J. *J. Organomet. Chem.* **1988**, 354, 7.

(30) Spaniol, A. Ph.D. Dissertation, University of the Saarland, Saarbrücken, W. Germany, 1988; Veith, M. Private communication, 1989.

(31) Veith, M. *Chem. Rev.* **1990**, 90, 3.

(32) Jutzi, P. Private communication, 1989.



the bulky organic moieties prevents the indiums from getting closer together.

For indium there also exist two indium-indium bonded molecules with In in the formally +II oxidation state: I(Br)-In^{II}In^{II}Br₂·2(N,N,N',N'-tetramethylethanediamine) and [(Me₃Si)₂CH]₂In^{II} consist of discrete molecules with indium-indium bond lengths of 277.5⁴⁴ and 282.8 pm.⁴⁵

We note that the exotic aluminum(+I)⁴⁶ and the gallium(+I) oxidation states do not show the metal-metal interactions seen in some of the molecular complexes of their heavier congeners. To our knowledge, the only stable molecular Ga^I compounds are the arene-coordinated species (arene)₁₋₃Ga^I(μ-Cl)Ga^{III}Cl₃.⁴⁷ However, Ga-Ga bonding can be found in [X₃Ga^{II}-Ga^{II}X₃]²⁻ anions (X = Cl, Br, I) and in the 1,4-dioxane and pyridine adducts of Ga₂^{II}X₄ (X = Cl, Br)⁴⁸ as well as in [(Me₃Si)₂CH]₂Ga^{II}.⁴⁹ An Al-Al bond is observed in K₂[i-Bu₃Al^{II}-Al^{II}i-Bu₃] and in Al₂^{II}i-Bu₄⁵⁰—although structurally authenticated only in [(Me₃Si)₂CH]₂Al^{II}]₂⁵¹ (oxidation states were assigned formally).

Solid-State Complexes

Examples of Tl...Tl and In...In contacts of the one-valent metals in the solid state are summarized in Table II.

Much shorter Tl^I-Tl^I or In^I-In^I distances can be found in solid-state compounds than in molecular complexes, as is evident from the examples in Tables I and II. The shortest M-M contacts given in Table II are 323 pm in Tl₂SnO₃⁹¹ and 262 pm in In₁₁-Mo₄₀O₆₂.⁵⁷ These distances, and some others, are well below the shortest separations seen in Tl or In metal³ (shortest Tl-Tl = 343.8 pm in hexagonal close packed, 336.2 pm in body centered cubic lattice; shortest In-In = 324 pm in distorted close packed cubic lattice).

On the basis of structural arguments, some authors assign M-M bonding interactions to short Tl-Tl or In-In contacts.^{43,52,56,57,75} Perhaps the most striking of these is a Tl^{II}-Tl^{II} distance of 284 pm, argued convincingly to correspond to a single bond in the Tl₂⁴⁺ pairs in Tl_{0.8}Sn_{0.6}Mo₇O₁₁.⁹⁵ The divalent thallium ions in these pairs are displaced toward each other from the central positions of irregular face-sharing oxygen polyhedra (see 22).

We note that the short In^I-In^I contacts fall in the same range as In^{II/III}-In^{II/III} distances found in solid-state compounds,^{45,57} e.g. 280/277, 282 pm in InS/Se,⁹⁶ 274/276 in In₄S₇/Se₇,⁹⁷ 277/278 in In₄Se₃/Te₃,^{58,98} 277 in In₅S₄,⁹⁹ 269 and 272 in In₂Br₃,⁶⁸ and 267-274 pm in In₅Br₇.¹⁰⁰

- (44) Khan, M. A.; Peppe, C.; Tuck, D. G. *Can. J. Chem.* **1984**, *62*, 601.
 (45) Uhl, W.; Layh, M.; Hiller, W. *J. Organomet. Chem.* **1989**, *368*, 139.
 (46) Cotton, F. A.; Wilkinson, G. In *Advanced Inorganic Chemistry*, 5th ed.; Wiley: New York, 1988; p 229.
 (47) (a) Schmidbauer, H.; Haager, R.; Huber, B.; Müller, G. *Angew. Chem.* **1987**, *99*, 354; *Angew. Chem., Int. Ed. Engl.* **1987**, *26*, 338. (b) Schmidbauer, H. *Ibid.* **1985**, *97*, 893; **1985**, *24*, 893.
 (48) (a) Brown, K. L.; Hall, D. J. *Chem. Soc. Dalton* **1973**, 1843. (b) Cumming, H. J.; Hall, D.; Wright, C. E. *Cryst. Struct. Commun.* **1974**, *3*, 107. (c) Small, R. W. H.; Worrall, I. J. *Acta Crystallogr.* **1982**, *B38*, 86, 250. (d) Beamish, J. C.; Small, R. W. H.; Worrall, I. J. *Inorg. Chem.* **1979**, *18*, 220. (e) Khan, M. A.; Tuck, D. G.; Taylor, M. J.; Rogers, D. A. *J. Crystallogr. Spectrosc. Res.* **1986**, *16*, 895.
 (49) Uhl, W.; Layh, M.; Hildenbrand, T. *J. Organomet. Chem.* In press.
 (50) (a) Hoberg, H.; Krause, S. *Angew. Chem.* **1978**, *90*, 1013; *Angew. Chem., Int. Ed. Engl.* **1978**, *17*, 949. (b) Miller, M. A.; Schram, E. P. *Organometallics* **1985**, *4*, 1362.
 (51) Uhl, W. *Z. Naturforsch.* **1988**, *43b*, 1113.
 (52) Fleet, M. E. *Z. Kristallogr.* **1973**, *138*, 147.
 (53) Blacknik, R.; Dreisbach, H. A. *J. Solid State Chem.* **1984**, *52*, 53.
 (54) Jaulmes, S.; Houenou, P. *Mat. Res. Bull.* **1980**, *15*, 911.
 (55) Marchand, R.; Piffard, Y.; Tournoux, M. *C. R. Acad. Sci. Paris, Sér. C* **1973**, *276*, 177.
 (56) Del Bucchia, S.; Jumas, J.-C.; Philippot, E.; Maurin, M. *Rev. Chim. Minér.* **1981**, *18*, 224.
 (57) (a) Mattausch, H.; Simon, A.; Peters, E.-M. *Inorg. Chem.* **1986**, *25*, 3428. (b) Simon, A.; Mertin, W.; Mattausch, H.; Gruehn, R. *Angew. Chem.* **1986**, *98*, 831; *Angew. Chem., Int. Ed. Engl.* **1986**, *25*, 845.
 (58) Hogg, J. H. C.; Sutherland, H. H.; Williams, D. J. *Acta Crystallogr.* **1973**, *B29*, 1590.
 (59) Gastaldi, L.; Carré, D.; Pardo, M. P. *Acta Crystallogr.* **1982**, *B38*, 2365.
 (60) Ketelaar, J. A. A.; t'Hart, W. H.; Moerel, M.; Polder, D. *Z. Kristallogr.* **1939**, *101*, 396.
 (61) Hahn, H.; Klingler, W. *Z. Anorg. Chem.* **1949**, *260*, 110.
 (62) Schubert, K.; Dörre, E.; Kluge, M. *Z. Metallkunde* **1955**, *46*, 216.
 (63) Müller, D.; Eulenberger, G.; Hahn, H. *Z. Anorg. Allg. Chem.* **1973**, *398*, 207.
 (64) Deiseroth, H.-J.; Müller, D.; Hahn, H. *Z. Anorg. Allg. Chem.* **1985**, *525*, 163.
 (65) Müller, D.; Hahn, H. *Z. Anorg. Allg. Chem.* **1978**, *438*, 258.
 (66) Helmholz, L. *Z. Kristallogr.* **1936**, *95*, 129.

- (67) Stephenson, N. C.; Mellor, D. P. *Aust. J. Res.* **1950**, *3A*, 581.
 (68) Staffel, T.; Meyer, G. *Z. Anorg. Allg. Chem.* **1987**, *552*, 113.
 (69) Klepp, K.; Yvon, K. *Acta Crystallogr.* **1980**, *B36*, 2389.
 (70) Berger, R. A.; Sobott, R. *J. Monatsh. Chem.* **1987**, *118*, 967.
 (71) (a) Berger, R. *J. Solid State Chem.* **1987**, *70*, 65. (b) Berger, R. *Chem. Scr.* **1988**, *28*, 41.
 (72) Berger, R.; Meerschaut, A. *Eur. J. Solid State Inorg. Chem.* **1988**, *25*, 279.
 (73) Nilson, L.; Hesse, R. *Acta Chem. Scand.* **1969**, *23*, 1951.
 (74) Jennische, P.; Olin, Å.; Hesse, R. *Acta Chem. Scand.* **1972**, *26*, 2799.
 (75) McCarley, R. E.; Lii, K.-H.; Edwards, P. A.; Brough, L. F. *J. Solid State Chem.* **1985**, *57*, 17.
 (76) Klepp, K.; Boller, H. *Monatsh. Chem.* **1978**, *109*, 1049.
 (77) Berger, R. *J. Less-Common Met.* **1989**, *147*, 141.
 (78) Tédénac, J.-C.; Brun, G.; Maurin, M. *Rev. Chim. Minér.* **1981**, *18*, 69.
 (79) Klepp, K.; Boller, H.; Völlenkle, H. *Monatsh. Chem.* **1980**, *111*, 727.
 (80) Ihara, H.; Sugise, R.; Hayashi, K.; Terada, N.; Jo, M.; Hirabayashi, M.; Negishi, A.; Atoda, N.; Oyanagi, H.; Shimomura, T.; Ohashi, S. *Phys. Rev. B* **1988**, *38*, 11952.
 (81) Morosin, B.; Ginley, D. S.; Schirber, J. E.; Venturini, E. L. *Physica C* **1988**, *156*, 587.
 (82) Liang, J. K.; Zhang, Y. L.; Huang, J. Q.; Xie, S. S.; Che, G. C.; Cheng, X. R.; Ni, Y. M.; Jia, S. L. *Mod. Phys. Lett. B* **1989**, *3*, 561.
 (83) Hervieu, M.; Maignan, A.; Martin, C.; Michel, C.; Provost, J.; Raveau, B. *J. Solid State Chem.* **1988**, *75*, 212.
 (84) Liang, J. K.; Zhang, Y. L.; Huang, J. Q.; Xie, S. S.; Che, G. C.; Chen, X. R.; Ni, Y. M.; Zhen, D. N. *Z. Phys. B* **1988**, *73*, 9.
 (85) Liang, J. K.; Zhang, Y. L.; Rao, G. H.; Cheng, X. R.; Xie, S. S.; Zhao, Z. X. *Solid State Commun.* **1989**, *70*, 661.
 (86) Weis, J.; Schäfer, H.; Eisenmann, B.; Schön, G. *Z. Naturforsch.* **1974**, *29b*, 585.
 (87) Leclerc, B.; Bailly, M. *Acta Crystallogr.* **1973**, *B29*, 2334.
 (88) Ketelaar, J. A. A.; Gorter, E. W. *Z. Kristallogr.* **1939**, *101*, 367.
 (89) Sabrowsky, H. *Z. Anorg. Allg. Chem.* **1971**, *381*, 266.
 (90) Verbaere, A.; Dion, M.; Tournoux, M. *J. Solid State Chem.* **1974**, *11*, 60.
 (91) Verbaere, A.; Dion, M.; Tournoux, M. *J. Solid State Chem.* **1974**, *11*, 184.
 (92) Klepp, K. O. *Monatsh. Chem.* **1984**, *115*, 1133.
 (93) Eulenberger, G. *Z. Kristallogr.* **1977**, *145*, 427.
 (94) Klepp, K. O. *Z. Naturforsch.* **1984**, *39b*, 705.
 (95) Dronskowski, R.; Simon, A. *Angew. Chem.* **1989**, *101*, 775; *Angew. Chem., Int. Ed. Engl.* **1989**, *28*, 758.
 (96) (a) Schubert, K.; Dörre, E.; Günzel, E. *Naturwissenschaften* **1954**, *41*, 448. (b) Duffin, W. J.; Hogg, J. H. C. *Acta Crystallogr.* **1966**, *20*, 566. (c) Rigout, J.; Rimsky, A.; Kuhn, A. *Acta Crystallogr.* **1980**, *B36*, 916. (d) Likforman, A.; Carré, D.; Etienne, J.; Bachet, B. *Acta Crystallogr.* **1975**, *B31*, 1252.
 (97) (a) Hogg, J. H. C.; Duffin, W. J. *Acta Crystallogr.* **1967**, *23*, 111. (b) Hogg, J. H. C. *Acta Crystallogr.* **1971**, *B27*, 1630.
 (98) Hogg, J. H. C.; Sutherland, H. H. *Acta Crystallogr.* **1973**, *B29*, 2483.
 (99) Wadsten, T.; Arnberg, L.; Berg, J.-E. *Acta Crystallogr.* **1980**, *B36*, 2220.

Table II. Solid-State Structures with Tl^I-Tl^I or In^I-In^I Contacts Below 400 pm^a

formula	description of Tl/In Substructure	Tl-Tl/In-In/ppm ^b	ref	
Discrete Units				
Tl ₂ As ₂ S ₄	Tl-Tl pairs with each Tl 5-fold coordinated by S in a distorted square pyramid	354	52	
Tl ₃ Se ₂ I	Tl(2) pairs with each Tl having 3 Se and 2 I as nearest neighbors in an extremely distorted octahedron; antiprism of Tl(2) with Tl(1) in center, Tl(1)-Tl(2)	351 382	53	
Tl ₂ SnSe ₃	Tl(2) pairs with each Tl coordinated by 8 Se in a square antiprism, sharing a common base	343	54	
Tl ₃ BO ₃	6-membered Tl rings in a chair conformation	360 within rings	55	
Tl ₄ SnS ₃	Tl-Tl contact between 8-membered Tl-S rings and between sheets of these rings	385-386 between rings 357, 360 (×2)	56	
{(η ⁵ -C ₅ H ₅)In} _∞	infinite In-Cp-In-Cp zigzag chains with interstrand In...In contacts kinked In ₅ ⁷⁺ (=In ₂ ²⁺ In ₃ ⁺) and In ₆ ⁸⁺ (=In ₂ ²⁺ In ₄ ⁺) chain segments (In-In-In ~ 160°), middle In's square planar coordinated by 4O, top-to-bottom In ₅ ⁷⁺ -In ₆ ⁸⁺ distance	399	26, 43	
{(η ⁵ -MeC ₅ H ₄)In} _∞		399	43	
In ₁₁ Mo ₄₀ O ₆₂		262 (In ₅ ⁷⁺)	57	
		266 (In ₆ ⁸⁺)		
In ₄ Se ₃	In ⁺ pairs,	333	58	
= In ¹⁺ (In ₃ ⁵⁺)Se ₃ ²⁻	bent In ₃ units (∠ 157.8°)	344 276, 278		
In ₆ La ₁₀ O ₆ S ₁₇	In ^I pairs with each In 5-fold coordinated by S in a square pyramid	286	59	
Extended Structures—Chains				
TlSe = Tl ^I Tl ^{III} Se ₂	TlSe-type, see Figure 15, linear Tl ^I /In ^I chains with each Tl ^I /In ^I coordinated by 8 chalcogenides in a square antiprism; intrachain distances are between 550 and 600 ppm	350	60	
TlS = Tl ^I Tl ^{III} S ₂		340	61	
InTe = In ^I In ^{III} Te ₂		357	62	
TlGaTe ₂		342	63	
TlInSe ₂		342	63	
TlInTe ₂		359	63	
InGaTe ₂		344	64	
InGaSe ₂		316	64	
TlGaSe ₂	slightly kinked Tl chains (∠ ~ 176°) with each Tl coordinated by 6 Se in a trigonal prism	379-383	65	
TlI	interlayer contact in the form of a Tl/In zigzag chain	383	66	
InBr		368/355	67/68	
TlCu ₃ S ₂		Tl double chain	386 intrachain 385 interchain	69
TlCu ₇ S ₄ /Se ₄	Tl chain with each Tl coordinated by 8 S/Se in a tetragonal pseudocubic prism	386/397	70/71	
Tl ₃ Cu ₁₄ Se ₁₀	Tl triple chains	396 intrachain 391 interchain	72	
(C ₃ H ₇) ₂ NCS ₂ Tl	kinked chain with alternating ligand "bridged"/ "nonbridged" Tl-Tl contacts	398/400	73	
(i-C ₃ H ₇) ₂ NCS ₂ Tl		358/364	74	
InMo ₄ O ₆		linear In chains with each In coordinated by 4 O in a square plane	286	75
Two-Dimensional Nets				
TlFe ₂ S ₂ /Se ₂	ThCr ₂ Si ₂ -type structure, see Figure 24, planar-square Tl nets, sandwiched between chalcogenide nets, chalcogenides in 4-fold hollows of Tl nets, see 27	376/389	76	
TlCo ₂ S ₂ /Se ₂		374/385	76	
TlNi ₂ S ₂ /Se ₂		379/387	76	
TlCu ₂ S ₂ /Se ₂		378/385	77/76, 78	
TlCu ₄ S ₃ /Se ₃		KCu ₄ S ₃ -type, Tl square nets	389/397	78, 79
TlBa ₂ Ca ₃ Cu ₄ O ₁₁		square-planar Tl nets with each Tl at the center of an O octahedron	390	80
TlBa ₂ Ca ₂ Cu ₃ O ₉			385	81
TlBa ₂ Ca ₂ Cu ₃ O _{8.5}			385	82
TlBa ₂ CaCu ₂ O _{8.5}			383	83
TlBa ₂ CaCu ₂ O _{6.5}			385	84
TlSr ₂ Ca _{0.5} Sm _{0.5} Cu ₂ O _{6.75}		382	85	
TlTe	irregular Tl net	354, 371 (×2)	86	
Tl ₄ S ₃ = Tl ₃ ^I Tl ^{III} S ₃	irregular Tl net	346-377	87	
Tl ₂ S	sheets of 2 Tl layers sandwiching a chalcogenide layer, each Tl coordinated by 3 chalcogenides (shortest contacts are given)	350 in layer 1 372 in layer 2 360 between sheets 351 intra Tl layer 362 between sheets	88 89	
Tl ₂ O				
Three-Dimensional Frameworks				
Tl ₂ TiO ₃	linear Tl chain along c-direction plus 3 Tl in ab plane with similar distances; each Tl coordinated by 3 or 4 O in distorted triangular or square pyramid, depending on how many O are counted toward the Tl coordinated sphere	375 "intrachain" 366, 378, 381 "intrachain"	90	
Tl ₂ SnO ₃		323 "intrachain" 344, 353, 365 "interchain"	91	
Tl ₂ SnS ₃	slightly kinked chains of Tl(2) with each Tl coordinated by a cube of S; Tl(2) chains in contact with each other and with perpendicular linear chains of Tl(1) (coordinated trigonal prismatic by S)	368, 372 "intrachain" 383 "interchain" Tl(2) 383 "intrachain" Tl(1) 390 "interchain" Tl(1)-Tl(2)	92	

Table II (Continued)

formula	description of Tl/In Substructure	Tl-Tl/In-In/ppm ^b	ref
Tl ₄ GeS ₄	strongly distorted frame frame, built up from distorted Tl ₄ squares	345-390	93
Tl ₄ TiS ₄		251-380 intrasquare	94
Tl ₄ SnS ₄		382-398 intersquare	94
Tl ₄ TiSe ₄		346-378 intrasquare	94
		370-394 intersquare	94
		353-386 intrasquare	94
		384-391 intersquare	

^aThe description of the Tl/In substructure is quite formal. We do not mean to imply that the Tl/In contacts have any structural significance or even give rise to metal-metal bonding. ^bDistances abbreviated to nearest pm.

We tried to group the structures in Table II according to the predominant Tl/In substructure: isolated pairs, infinite chains, two-dimensional nets, or three-dimensional frameworks. This was done without implying that this formalistic feature has significance in all cases, or even that it is consistent with metal-metal bonding. It will be the object of our study to identify the cases where direct metal-metal interactions should be invoked. For some of the compounds listed in Table II physical property studies have been reported in the literature: acousto-optic properties for TlGaSe₂ and TlInSe₂,¹⁰¹ resistivity for TlCu₂Se₂ and TlCu₄Se₃,⁷⁸ electrical conductivity, photoconductivity, Hall effect for TlInSe₂/Te₂,^{102,103} and TlGaSe₂/Te₂,^{103,104} electrical conductivity and Hall effect for TlCu₂Se₂,^{77,105} electrical properties of single crystals of TlS and TlSe,¹⁰⁶ and conductivity measurements on InGaSe₂,⁶⁴ and In-Mo₄O₆.⁷⁵ Also, we note that a pseudopotential calculation of the band structure has been carried out for TlSe, InTe, TlInSe₂ and TlInTe₂, and TlGaS₂.¹⁰⁷

The Discrete Molecular State

For a preliminary communication of some of these results see ref 108. To analyze the possibilities for bonding between two formally closed subshell Tl⁺(s²) centers, we start with two naked Tl⁺ atoms at a distance of 370 pm. Judging from the examples listed in Tables I and II, this distance is typical of Tl...Tl contacts in molecular or solid-state compounds. We also note that relativistic effective potential (REP) SCF calculations give an equilibrium distance of ~370 pm for Tl₂⁰ (O_u⁻ ground state) and 384 pm for Tl₂⁺ (1/2_g ground state). If spin-orbit coupling is excluded, the minima of the potential curves range from about 300 to 380 pm for Tl₂⁰, depending on the ground state (³Σ_g⁻, ³Π_u, or ¹Σ_g⁺)¹⁸ with the lowest minimum at ~325 pm (³Π_u). However, a quasirelativistic model potential approach estimates the equilibrium distances between ~240 and 300 pm for Tl₂⁰,¹⁹ while an REP calculation with configuration interaction gave 354 pm for the ground state.²⁰ Tl₂ and Tl₂⁺ seem to be examples opposing the normally seen contractions in bond lengths upon inclusion of relativistic effects. In the case of Tl₂, Tl₂⁺ they effectively destroy the bond.²¹ The extended Hückel method is known not to give reasonable bond distances,¹⁰⁹ for example, Tl₂⁰ shows an orbital energy minimum at a separation of 140 pm and Tl₂²⁺ at 200 pm. This will preclude varying the distance in our calculations. We will fix the Tl-Tl separation and follow a bonding indicator that has proven more reliable, the overlap population.

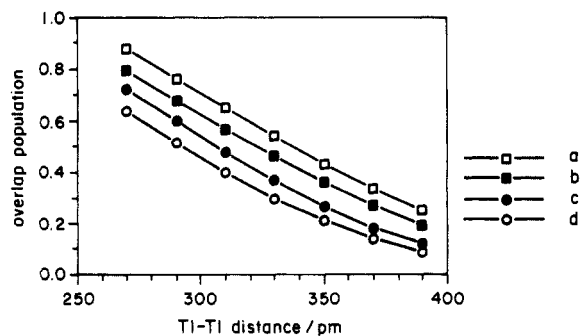
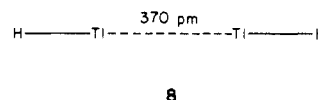


Figure 1. Orbital parameter and distance dependence of the overlap population illustrated for the example of the Tl^I-Tl^I dimer, Tl₂²⁺: (a) parameter set used in all subsequent calculations ($\zeta_{6s} = 2.30$, $\zeta_{6p} = 1.60$, $H_{6s} = -11.6$ eV, $H_{6p} = -5.8$ eV); (b) larger orbital energy difference, same Slater coefficients as in part a (2.30, 1.60, -12.8 eV, -5.1 eV); (c) s and p orbitals more contracted, same orbital energy as in part a (2.52, 1.77, -11.6 eV, -5.8 eV); (d) b and c combined (2.52, 1.77, -12.8 eV, -5.1 eV).

At first, we will consider only the interaction between the s orbitals or between the p orbitals on the two Tl⁺ centers. Then the s-p mixing will be turned on to demonstrate its effect and importance for the bonding interaction. Eventually, we will bring in two hydrogen ligands at opposite ends of the Tl-Tl axis at an angle of 180° (8). Finally, we will vary the H-Tl-Tl angle in the model complex HTl-TlH.



The justification for moving to a hydride ligand in place of a more realistic OR, or Te, or Cp, or (PhCH₂)₅C₅, is that we have actually done calculations for all of these (except the penta-benzylcyclopentadienyl) and the essential results are similar.

Since we will make much use of the theoretical concept of overlap population when referring to the bonding or antibonding character of orbitals, or to the bond strength between two atoms, a few words about this construct seem appropriate.^{110,111} The Mulliken overlap population between two atomic orbitals located on two atoms A and B in a molecule is $2c_i c_j S_{ij}$ for one electron. This corresponds to the amount of electron density transferred to the region between A and B upon interaction of the two atomic orbitals under consideration. Depending on the signs of the orbital coefficients c_i , c_j , the overlap population, representing the shared electron density of A + B, can be positive or negative. From much experience, a larger positive overlap population correlates with a stronger bond and a larger bond order between atoms A and B. However, actual numbers can only be compared within a related series, keeping the atom pair A,B constant. For example, the overlap population of a transition-metal-transition-metal bond should not be compared to that of a carbon-carbon bond. The orbital overlap (S_{ij}) term in the definition of the overlap population is different for different orbitals or atom pairs. Therefore, it is

(110) Albright, T. A.; Burdett, J. K.; Whangbo, M.-H. *Orbital Interactions in Chemistry*; Wiley-Interscience: New York, 1985.

(111) Hoffmann, R. *Solids and Surfaces: A Chemist's View of Bonding in Extended Structures*; VCH Verlagsgesellschaft: Weinheim, 1988.

(100) Staffel, T.; Meyer, G. Z. *Anorg. Allg. Chem.* **1988**, *563*, 27.

(101) Gottlieb, M.; Isaacs, T. J.; Feichtner, J. D.; Roland, G. W. *J. Appl. Phys.* **1974**, *45*, 5145.

(102) Guseinov, G. D.; Mooser, E.; Kerimova, E. M.; Gamidov, R. S.; Alekseev, I. V.; Ismailov, M. Z. *Phys. Status Solidi* **1969**, *34*, 33.

(103) Guseinov, G. D.; Ramazanzade, A. M.; Kerimova, E. M.; Ismailov, M. Z. *Phys. Status Solidi* **1967**, *22*, K117.

(104) Karpovich, I. A.; Chervova, A. A.; Demidova, L. I.; Leonov, E. I.; Orlov, V. M. *Izv. Akad. Nauk, SSSR, Neorg. Mater.* **1972**, *8*, 70.

(105) Berger, R.; van Bruggen, C. F. *J. Less-Common Met.* **1984**, *99*, 113.

(106) (a) Hussein, S. A.; Nagat, A. T. *Cryst. Res. Technol.* **1989**, *24*, 283. (b) Hussein, S. A. *Ibid.* **1989**, *24*, 467. (c) Hussein, S. A.; Nagat, A. T.; Mohamed, N. M. *Ibid.* **1989**, *24*, 685. (d) Nagat, A. T. *Ibid.* **1989**, *24*, K113.

(107) (a) Gashimzade, F. M.; Orudzhev, G. S.; Nizametdinova, M. A. *Fiz. Svoistva Slozhnykh Poluprovodn.* **1982**, *80*; *Chem. Abstr.* **100**: 197979p. (b) Abdullaeva, S. G.; Mamedov, N. T.; Orudzhev, G. S. *Phys. Status Solidi* **1983**, *119b*, 41.

(108) Janiak, C.; Hoffmann, R. *Angew. Chem.* **1989**, *101*, 1706; *Angew. Chem., Int. Ed. Engl.* **1989**, *28*, 1688.

(109) Hoffmann, R. *J. Chem. Phys.* **1963**, *39*, 1397.

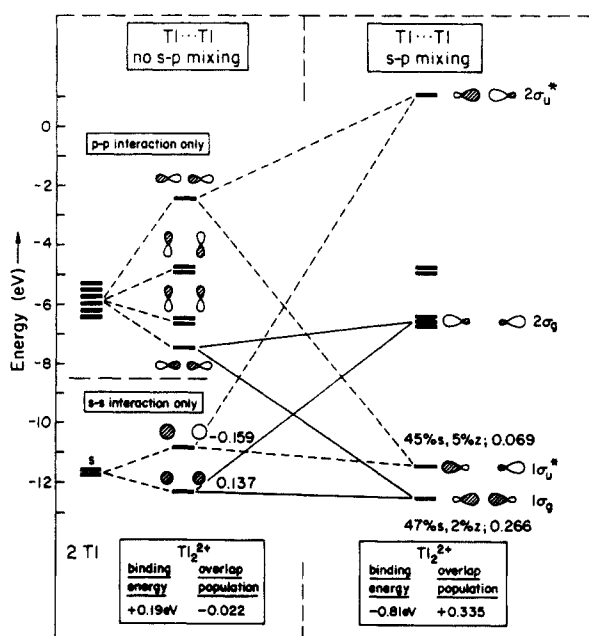


Figure 2. Interaction diagram for two thallium atoms at a distance of 370 pm. The hybrid orbital sketches are exaggerated for clarification. Numbers at levels refer to the respective orbital overlap population. A positive binding energy indicates repulsion, a negative value attraction.

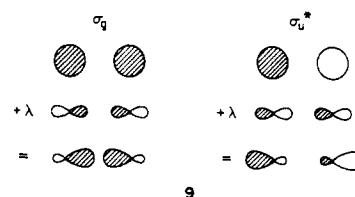
not so much the single, absolute number that is meaningful but the trend that is observed upon the variation of geometrical and electronic factors.

In this context another *caveat* is in place: The numerical values for the overlap populations that we are going to report in the following correlate with s - p hybridization, which in turn depends of course on the orbital parameters (energy, exponents; see Appendix) we use in our calculations. Employing a different set of parameters may give different numerical values. However, general trends like the variation of the overlap population with the ligand-metal core geometry of ligand character should be preserved. In the following, we do not specifically elaborate on the parameter sensitivity of our results. In general though, larger Slater exponents (ζ) for a given element make the orbitals more contracted, thereby decreasing any hybridization effects (other things being equal). Increasing the orbital energy difference ($H_{ss} - H_{pp}$) operates in the same direction. These trends are illustrated in Figure 1 over a distance range for the example of the Tl_2^{2+} dimer discussed below.¹¹²

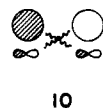
The Interaction of Two Tl(I) Centers. If one allows only 6s orbitals on Tl^+ , then the situation depicted in the lower left part of Figure 2 is obtained. The computed binding energy indicates repulsion, and the overlap population is negative. This is due to the fact that the extended Hückel method calculates the antibonding molecular orbitals to be more destabilized than the bonding ones are stabilized, relative to the 6s orbitals on an isolated Tl atom. Looking at the (empty) 6p orbitals alone, a similar splitting pattern is found. Therefore the net effect from solely s^2 - s^2 interaction for Tl_2^{2+} is antibonding.

However, when s - p mixing is allowed, as it must be, drastic changes are apparent. The right part of Figure 2 illustrates the interaction of the symmetry-allowed (s - s)-bonding with the (z - z)-bonding (we use the notation hereafter of $z \equiv p_z$) and the (s - s)*-antibonding with the (z - z)*-antibonding combination. The σ_g and σ_u^* from the 6p mix into the occupied 6s combinations with the same symmetry, in such a way as to stabilize the 6s σ_g and σ_u^* orbitals. This is represented schematically in 9.

The main effect of such interaction is the lowering in energy of the $1\sigma_u^*$ orbitals and its transformation from a strongly s - s antibonding into an s - s nonbonding orbital. The $1\sigma_u^*$ can be



thought of as moving toward a lone-pair combination. It even has a slightly positive overlap population. This is due to the z_1-s_2/s_1-z_2 cross terms, as shown in 10.



The 1σ orbital also becomes more bonding. Overall, the initially closed-subshell repulsion changes into an attraction for Tl_2^{2+} , by inclusion of unfilled orbitals of proper symmetry. This is a general phenomenon and can also be seen in d^{10} - d^{10} systems, such as Cu^I - Cu^I ,¹¹³ Pt^0 - Pt^0 ,¹¹⁴ Au^I - Au^I ,¹¹⁵ etc. We would like to point out that even though the mixing between the s and p combinations in the thallium dimer appears numerically quite small, it nevertheless has a substantial effect.

The basic result of a principally bonding overlap population for Tl_2^{2+} (or Tl_2^0) is in agreement with REP calculations mentioned earlier. It was found in these calculations that Tl_2^+ is more strongly bonded (dissociation energy, $D_e = 0.58$ eV for an equilibrium distance, $R_e = 384$ pm)¹⁸ than the neutral Tl_2^0 ($D_e = 0.16$ eV, $R_e = 354$ pm),²⁰ although this phenomenon is not yet understood. An experimental study gave a dissociation energy of 0.63 eV for Tl_2^0 ; however, a bond length of 276 pm was assumed.¹⁶ It is also interesting that Tl_2^+ could be observed in photoionized high-temperature vapors of thallium fluoride.¹⁵ At this point, we have to acknowledge that the binding energies from the extended Hückel method cannot be compared to the above dissociation energies. We compute a binding energy of -1.32 eV for Tl_2^+ at $d = 384$ pm. This could be partly due to the atomic parameters we use for thallium, which are not yet widely checked. Also, the extended Hückel method is not able to reproduce the trend of Tl_2^+ being more strongly bonded than Tl_2^0 . It would rather predict the reverse—as can easily be seen from Figure 2: The degenerate π set at -6.42 eV, which would be filled with one or two electrons in the case of Tl_2^+ or Tl_2^0 , has some bonding character. This is truly a limitation of the method, which does not take into account many-electron or relativistic effects nor spin-orbit coupling.

The Tl_2^{2+} species can be considered part of an isoelectronic series of s^2 - s^2 interacting dimers such as Be_2 ,^{116a-c} K_2^{2-} , and Rb_2^{2-} .^{116d-f} Some infinite Rb^- and Cs^- chains have also been observed in alkalides,^{116e,f} which would correspond to the Tl^+ chains discussed later.

The Role of Terminal (Hydrogen) Ligands. In order to understand the influence of terminal ligands on the orbitals of the Tl - Tl system, the simplest ligand possible, a hydrogen atom, is bonded to each thallium at opposite ends along the Tl - Tl axis, as depicted above in 8. The thallium-hydrogen bond was estimated at 190 pm from the sum of the covalent radii of thallium (152 pm) and hydrogen (37 pm). We note that experimental studies for TlH give an equilibrium distance of 187 pm,¹⁴ in good agreement with relativistic ab initio SCF calculations, where the results range from 179 to 199 pm,^{17b,21,22,117} depending on the

(112) We thank Dr. Gordon Miller for bringing another parameter set to our attention based on work by T. Hughbanks (see Appendix, ref 142) ($\zeta_{6s} = 2.52$, $\zeta_{6p} = 1.77$, $H_{6s} = -12.8$ eV, $H_{6p} = -5.1$ eV).

(113) (a) Mehrotra, P. K.; Hoffmann, R. *Inorg. Chem.* **1978**, *17*, 2187. (b) Merz, K. M.; Hoffmann, R. *Inorg. Chem.* **1988**, *27*, 2120. (114) Dedieu, A.; Hoffmann, R. *J. Am. Chem. Soc.* **1978**, *100*, 2074. (115) Jiang, Y.; Alvarez, S.; Hoffmann, R. *Inorg. Chem.* **1985**, *24*, 749. (116) (a) Bondybey, V. E. *Chem. Phys. Lett.* **1984**, *109*, 436. (b) Røeggen, I.; Morokuma, K.; Yamashita, K. *Chem. Phys. Lett.* **1987**, *140*, 349. (c) Painter, G. S.; Averill, F. W. *Phys. Rev. B* **1987**, *35*, 7713. (d) Huang, R. H.; Ward, D. L.; Dye, J. L. *J. Am. Chem. Soc.* **1989**, *111*, 5707. (e) Huang, R. H.; Ward, D. L.; Kuchenmeister, M. E.; Dye, J. L. *J. Am. Chem. Soc.* **1987**, *109*, 5561. (f) Dye, J. L.; DeBacker, M. G. *Annu. Rev. Phys. Chem.* **1987**, *38*, 271.

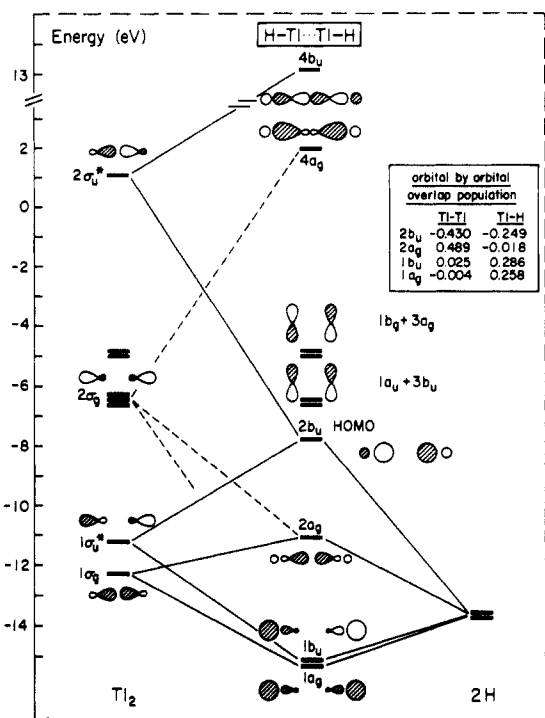
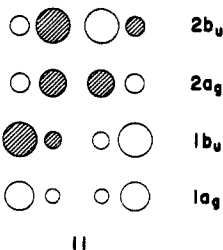


Figure 3. Molecular orbital diagram for HTl-TlH (8). Symmetry labels are for C_{2h}; relative orbital representations are schematic and hybridization is exaggerated for clarification.

method, effective core potential, configuration, etc. used. As for Tl₂⁰, the interest in TlH arises from the study of relativistic effects.

The hydrogen molecular orbitals interact mainly with the 1σ_g and 1σ_u* from the Tl₂²⁺ fragment, to give four filled orbitals of 1a_g, 1b_u, 2a_g, and 2b_u symmetry, which are shown in Figure 3. (The symmetry labels are assigned even here in C_{2h} point group symmetry, rather than D_{∞h}. This anticipates the trans-bending we will soon study.) The two lowest filled orbitals, 1a_g and 1b_u, are mostly hydrogen based and H-Tl bonding in character, while the two highest filled orbitals, the HOMO (2b_u) and the HOMO-1 (2a_g), are mainly thallium based. There is of course also an important interaction of the hydrogen s orbitals with the 2σ_g and 2σ_u* combination on the Tl₂²⁺. The 2σ_g and 2σ_u* mix into the 2a_g and 2b_u, in what can be considered a second-order mixing. As a result the 2a_g becomes more bonding—enhancing the effect of the first s-z mixing—while the 2b_u gets strongly antibonding again, the effect of the first mixing being canceled. The 2b_u HOMO is left with 1% z of “opposite” sign, so as to increase the antibonding 1σ_u* character.

The small contribution of z to 2b_u worried us at first, so we thought about explaining it from another perspective. Consider first allowing interaction between Tl s and H s orbitals and then turning on Tl p mixing. 11 shows the typical butadienoid orbital pattern from the first step. The coefficient size pattern is modified



by the different electronegativities of Tl and H. These orbitals will become 1a_g, 1b_u, 2a_g, and 2b_u of Figure 2.

(117) (a) Pyykkö, P.; Desclaux, J. P. *Chem. Phys. Lett.* **1976**, *42*, 545. (b) Lee, Y. S.; Ermier, W. C.; Pitzer, K. S. *J. Chem. Phys.* **1980**, *73*, 360. (c) Christiansen, P. A.; Pitzer, K. S. *J. Chem. Phys.* **1980**, *73*, 5160. (d) Pitzer, K. S.; Christiansen, P. A. *Chem. Phys. Lett.* **1981**, *77*, 589. (e) Christiansen, P. A.; Balasubramanian, K.; Pitzer, K. S. *J. Chem. Phys.* **1982**, *76*, 5087.

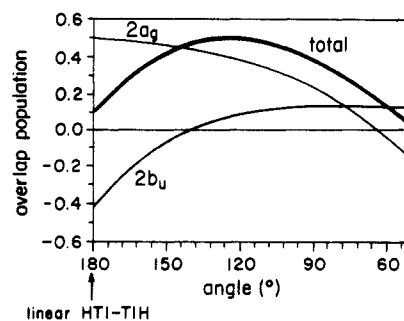
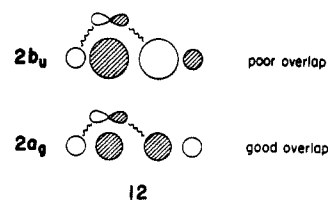


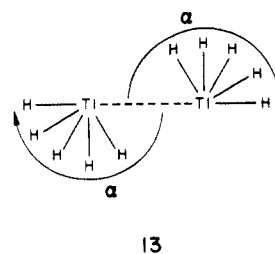
Figure 4. Overlap population-angle dependence for 13 with Tl-Tl = 370 pm and Tl-H = 190 pm.

In the next stage let us mix in p on Tl. The nodal pattern of the butadienoid orbitals is such that only 2a_g and 1b_u allow large p mixing, while 1a_g and 2b_u have, so to speak, the wrong pseudosymmetry to benefit from such mixing. This is shown for 2a_g and 2b_u in 12; in each case the admixed z orbital is displaced for clarity a bit off the Tl center.



The net result of these orbital interactions is that 2a_g is strongly Tl-Tl bonding, 2b_u Tl-Tl is antibonding (and Tl-H antibonding), and 1b_u and 1a_g contribute only to Tl-H bonding.

The Effect of the Angle Variation. The pentabenzylcyclopentadienyl ligands in {(PhCH₂)₅C₅Tl}₂ (3, 4) are placed at an angle with respect to the Tl...Tl axis, in a trans-bent geometry. This suggested an angle variation study of the HTl-TlH model compound, as depicted in 13. The results are quite surprising.



The bridged structures (1, Table I) can also be interpreted as being a point far along such a trans-bending trajectory, slightly readjusted so as to move the ligands into symmetrical bridging positions. Unfortunately, hydrogen does not lend itself to the study of the bridging extreme. At an H-Tl bond length of 190 pm, symmetrical bridging would place the hydrogens 86 pm apart from each other (cf. the molecular H₂ bond length of 74 pm), giving rise to strong H-H and unreasonable Tl...Tl interaction.

Plotting the overlap population between the Tl atoms in HTl-TlH as a function of the H-Tl-Tl angle in Figure 4 shows an increase upon bending, then a relatively large maximum at around 120°, and eventually a decline toward the bridging geometry. Both the magnitude and the range of variation are extraordinary. Thus, from an almost nonbonding situation in the linear arrangement, one passes over a region of strong bonding to again reach a nonbonding interaction.¹¹⁸ The latter extreme is in agreement with the general assumption in the literature that the bridged species do not display any Tl...Tl interactions.

Insight into this large variation is gained from an orbital-by-orbital decomposition of the overlap population. The major contributions from the HOMO (2b_u), and the one below the highest occupied MO (HOMO-1, 2a_g), are included in Figure 4.

(118) This conclusion is also reached by F. Wagner in his Diplomarbeit (Master-Thesis), Universität Erlangen-Nürnberg, West Germany, 1989.

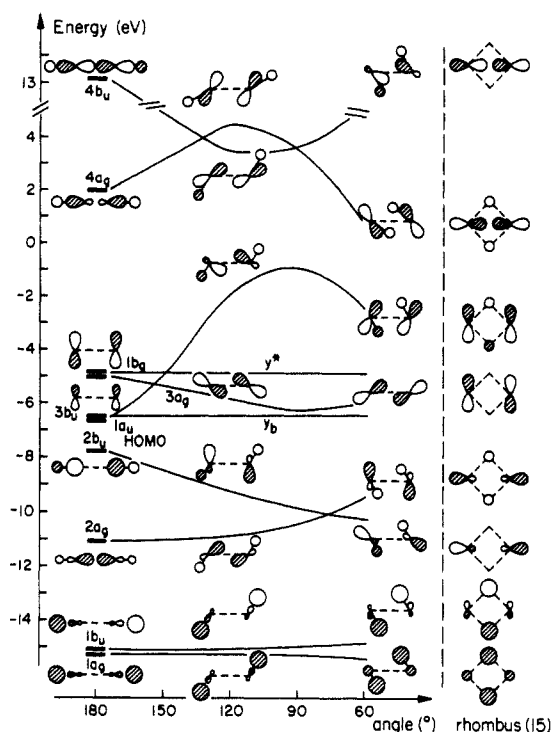


Figure 5. Walsh diagram for the bending in HTI...TIH (**13**), with TI-TI = 370 pm. Orbital sketches for the hypothetical Tl₂H₂ rhombus (**15**) are at the right-hand side. Symmetry labels are for point group C_{2h}; orbital drawings are schematic.

From the slope of the curves, it is obvious that from 180° to 120° the 2b_u orbital dominates the changes in the overlap population, while from 120° to 60°, the 2a_g is the governing factor. The relevant Walsh diagram (orbital energy vs angle) for HTI-TIH is given in Figure 5. Specific orbital pictures are given at α = 180°, 120°, and 60°.

At 180°, the orbital sketches are, of course, the ones we have just finished constructing in the bonding analysis of the linear HTI-TIH model complex. The Walsh diagram will be discussed in two steps or two segments: from 180° to 120° and from 60° to 120°.

In the range from 180° to 120° the most important changes among the filled levels involve the HOMO, 2b_u orbital. The 3b_u orbital, an initially x (x ≡ p_x) bonding combination, which has the same symmetry, mixes into the HOMO at angles smaller than 180°. (As pointed out above, at exactly 180° the symmetry is higher, D_{∞h}, and because of additional σ_v operations "3b_u" and "2b_u" are of different symmetry, therefore ruling out mixing.) The 2b_u-3b_u mixing, which pushes both levels apart, is responsible for changing the character of the 2b_u level from strongly antibonding to nonbonding and even slightly bonding (see Figure 4).

The important orbital interactions in the pyramidalization of AH₃ systems (e.g. NH₃, CH₃⁻, PR₃) and the bending of AH₂ molecules^{110,119} (e.g. H₂O, H₂S) are closely related to what happens in H-TI-TI-H bending. Let us review the essentials of the long and interesting story of these fascinating molecular deformations, sketched in **14**.



The controlling orbital for both AH₃ and AH₂ pyramidalization is an a₁ lone pair centered on the A atom, which decreases in energy with bending, mixing in more s character, and a hydrogen contribution as well. The lone pair begins as pure p in the planar

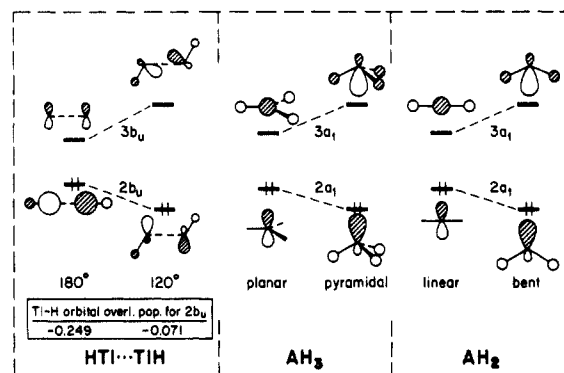


Figure 6. Analogy in the orbital diagram for the bending of HTI-TIH to AH₃ and AH₂ systems.

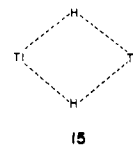
or linear geometry. When the sources of this frontier orbital stabilization are sought, they are found in a mixing with an A-H σ* orbital above and a corresponding σ orbital below. The former dominates, and it (3a₁) as well as the lone pair (2a₁) are shown in the right-hand panels of Figure 6. The left-hand panel of Figure 6 shows the corresponding orbitals of the HTI-TIH system, 2b_u and 3b_u. They play a role quite analogous to 2a₁ and 3a₁ in AH₃ and AH₂. In each case the lower, stabilized orbital is A-H (TI-H) nonbonding. The closer in energy the higher σ* combination to the p orbital in AH₃ or AH₂ is the stronger the tendency to bend. The only difference (in the undistorted structures) is that in the TI case the upper orbital (3b_u) is of TI p character, whereas in AH₃ and AH₂ it is the lower orbital. As soon as bending, therefore mixing, begins, this distinction becomes unimportant.

While the 2b_u mixes very strongly with the 3b_u (x bonding) combination in the 180° to 120° range, thereby transforming its character from strongly antibonding to slightly bonding, the main TI-TI bonding orbital, 2a_g, shows only very little interaction with orbitals of the same symmetry (e.g. x antibonding 3a_g) in this range. It thus retains its strongly bonding character. The difference in the mixing behavior of 2a_g and 2b_u can be explained by the larger energy gap between 2a_g and 3a_g versus 2b_u and 3b_u. In general the energy difference between two levels is one of the factors that influences the strength of its interactions—the smaller the gap, the more likely a strong mixing.

Another way of thinking about this mixing, governed by orbital energies, is that it provides the opportunity for a stereochemically active lone pair. By allowing the RTI...TIR molecule to bend, we give it the freedom to mix in more p to alter the (repulsive) character of the s²-s² combinations.

Summarizing the discussion of the 180°-120° segment of the Walsh diagram in Figure 5, we conclude that the maximum TI-TI overlap population should lie at the 120° angle.

In the α = 120° to 60° range interactions and changes seem slightly more complicated to pinpoint, partly due to the fact that a high symmetry structure, a departure point for a distortion at either end, does not exist. As mentioned above, geometrical constraints proscribe a reasonable bridging position for the hydrogens. However, for the sake of argument, we will assume that such a symmetric Tl₂H₂ rhombus (**15**) exists at some unspecified TI-H and TI-TI distance. We will then discuss the principal features of its orbital pattern, analyzing the initial energy slope upon angular distortion.



The orbitals and their approximate energies for **15** (sketched at the right edge of Figure 5) can be generated upon extrapolating from the given orbital scheme at α = 60°. Its TI-H antibonding character puts 2a_g at higher energy than 2b_u in **15**. Both 2a_g and 2b_u can be considered as lone-pair combinations, with only a small

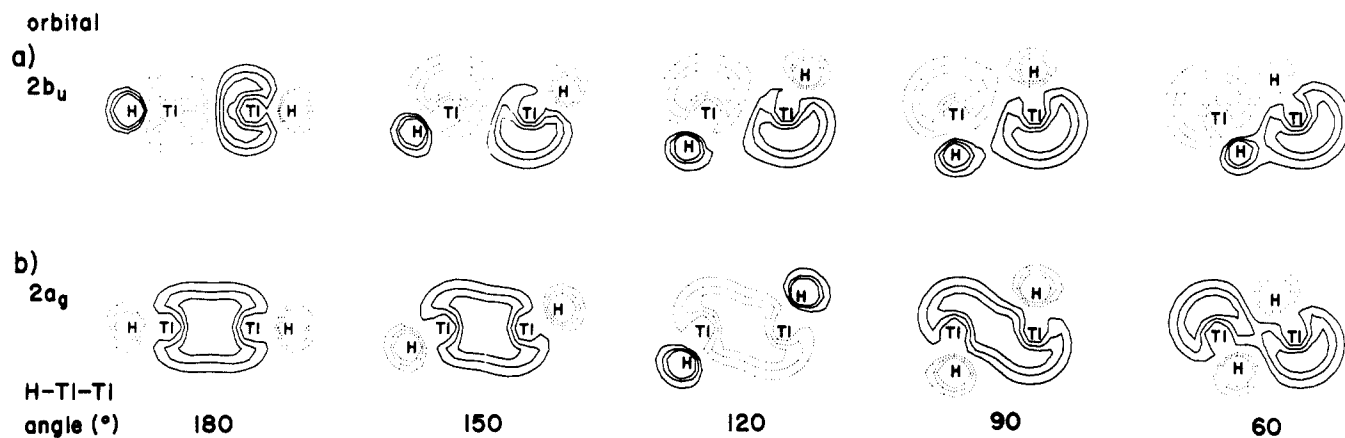


Figure 7. Contour diagrams for the two highest filled orbitals, $2b_u$ (a) and $2a_g$ (b), in HTITIH, following the H-Tl-Tl angle variation in **13**. Contour lines of ψ are ± 0.02 , 0.035 , and 0.05 .

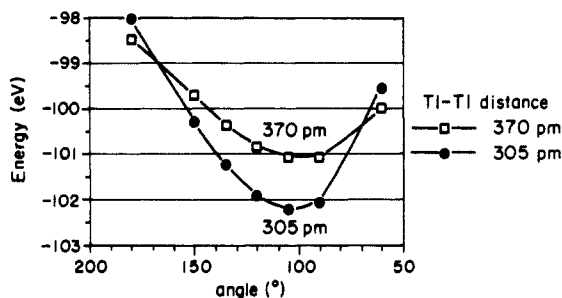


Figure 8. Energy as a function of the bending angle in HTI-TIH (**13**) at two Tl-Tl distances.

overlap population between the thalliums. Due to the important s - z cross terms, $2b_u$ will be slightly bonding, while $2a_g$ will be slightly antibonding in character. As in the linear HTI-TIH complex, symmetry prevents the interaction of the Tl x and y ($y \equiv p_y$) orbitals with z and s in **15**, but the Tl x levels can interact with hydrogen combinations of the appropriate symmetry.

Consider the initial slopes of $2b_u$ and $2a_g$ in **15** upon distortion: In the symmetrical case $2b_u$ ($2a_g$) is closest in energy to $1b_u$ ($3a_g$), among orbitals of the same symmetry. This gives the strongest (repulsive) interactions with them, for small perturbations. Such a repulsive interaction will raise the energy of $2b_u$, while lowering that of $2a_g$. The interaction of $2a_g$ with $3a_g$ (and eventually with $4a_g$) will change the character of $2a_g$ from a nonbonding or even slightly antibonding lone-pair combination into a more bonding s - s type and finally an sp - sp type interaction, thus steadily increasing the overlap population from **15** over 120° and beyond. Figure 7b shows the contour diagram for orbital $2a_g$, helping us to visualize these changes. $2b_u$ at the same time retains pretty much its nonbonding or slightly bonding character; the perturbation up to 120° is shown in Figure 7a. Put together, this rationalizes the maximum of the overlap population at 120° .

The energy minimum upon angle variation in **13** at 370 pm is observed around 105° (Figure 8). Given the simplified ligand, this is not too far from the observed geometry of **3**.

We note that the trans-bent ligand geometry is the arrangement that minimizes the total energy and maximizes the Tl-Tl and Tl-H overlap populations with respect to the H-Tl-Tl-H dihedral angle. Rotating one H out of the plane formed by the other three atoms destabilizes the system and decreases the Tl-Tl overlap population toward a minimum at a cis-bent geometry.

The Effect of the Tl...Tl Distance and the Relationship to H₂AAH₂ (3**) Systems.** Until now we have only studied the HTI-TIH system at a fixed distance of 370 pm. It is, of course, no surprise that at shorter separations the overlap population will increase. However, things are a little bit more complicated: A shorter distance also means an increased splitting between bonding levels and their antibonding counterparts. Thus the antibonding $2b_u$ orbital in Figures 3 or 5 will be pushed up, while the degenerate

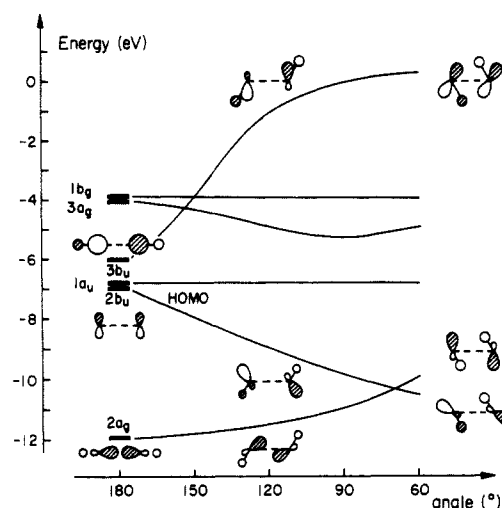


Figure 9. Partial Walsh diagram for the bending in HTI-TIH, with Tl-Tl = 305 pm. Symmetry labels are for C_{2h} ; orbital sketches are schematic.

bonding π -combination $3b_u + 1a_u$ will be lowered in energy. The $2b_u$ and $3b_u$ level will not cross because they are of the same symmetry, but at some distance smaller than 370 pm, they will change character. That means the x bonding combination will become $2b_u$, while the Tl-H s all-antibonding orbital will be the higher energy $3b_u$ at 180° . Thus, the orbital energy ordering at 180° at a Tl-Tl distance of let us say 305 pm (Figure 9) approaches the ordering seen in linear HAAH systems (where A = C, N, O),¹¹⁹ namely $2\sigma_g < 1\pi_u < 1\pi_g < 2\sigma_u$. A Tl...Tl separation of 305 pm was estimated as a reasonable bonding distance from the sum of the covalent radii.

The Walsh diagrams for **13** at Tl-Tl distances of 370 and 305 pm still look very similar, except that $2b_u$ and $3b_u$ start out being of different character at 180° . But due to the mixing between them, at angles smaller than 180° the $2b_u$ at 305 pm becomes almost like the $2b_u$ at 370 pm. This is especially so at angles lower than 120° (see orbital sketches in Figure 9). However, since the $2b_u$ orbital at 305 pm now starts out as a Tl-Tl (π) bonding combination, the change of the overlap population with angle is quite different from that seen at 370 pm (compare Figures 4 and 10). Figure 10 demonstrates that a local maximum for the total overlap population is no longer observed at 305 pm, instead it shows a maximum at 180° and then declines steadily. This is due to a change in the overlap population-angle dependence for the $2b_u$ orbital between 180 and 120° . The curvature for the $2a_g$ level does not show any differences, except for the expected generally larger overlap population values.

Also included in Figure 10 are the respective curves for the related system H₂Sn-SnH₂ (**6**) (calculated by us) to demonstrate part of the relationship between HTI-TIH and H₂Ge-GeH₂,

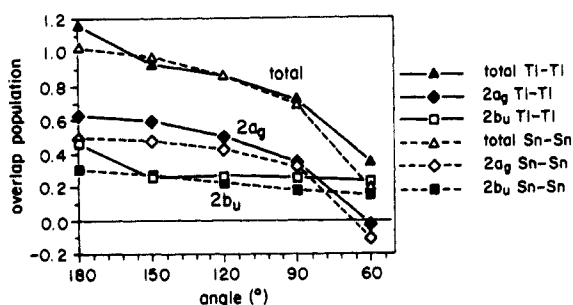
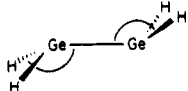


Figure 10. Overlap population-angle dependence for HTI-TIH, with TI-TI = 305 pm and H₂Sn-SnH₂ with Sn-Sn = 276 pm, Sn-H = 170 pm, H-Sn-H = 105°.

Table III. Comparison between Extended Hückel and ab Initio Results for H₂Ge-GeH₂^a



orbital symmetry	Extended Hückel		Ab-initio ^b	
	180	150	180	146
3a _g (LUMO)	-7.67 ↘	-7.93	+1.13 ↘	+0.46
2b _u (HOMO)	-9.95 ↘	-10.26	-7.22 ↘	-7.54
2a _g	-13.41 ↗	-13.26	-11.98 ↗	-11.69
1b _g	-14.77 ↗	-14.76	-12.99 ↗	-12.77
1a _u	-14.94 ↗	-14.95	-13.70 ↗	-13.50
1b _u	-18.12 ↗	-18.10	-17.78 ↗	-17.71
1a _g	-19.58 ↗	-19.60	-20.49 ↗	-20.39

angle with minimum energy: 133° (Extended Hückel), 146-140°^c (Ab-initio)

^aDistances for extended Hückel calculations: Ge-Ge = 235 pm, H-Ge = 153 pm, H-Ge-H = 110°. ^bAb initio data from ref 37. ^cRange from various ab initio studies, see refs 34, 37, and 38.

H₂Sn-SnH₂. The orbital pattern of HTI-TIH at 305 pm and its changes upon bending are closely related to the orbital diagram of H₂AAH₂ (A = Ge, Sn) if one ignores the additional A-H bond that breaks the degeneracy of the π-set at 180°.^{110,119}

We note that an extended Hückel MO calculation on digermylene at 180° and 150° correlates very well with the results of an ab initio calculation at 180° and 146°.³⁷ Both predict the same energy ordering of the orbitals and almost always the same initial slope (arrows in Table III), even if the absolute numbers are different. A comparison is presented in Table III. Also, the angle for the energy minimum from both methods is not too different.

The fact that the results for HTI-TIH at 305 pm match the results already in the literature for H₂A-AH₂ (A = Ge, Sn), as far as qualitative Walsh diagrams and overlap populations are concerned, gave us some confidence in the thallium parameters.

The energy minimum for the bending of HTI-TIH at 305 pm was found around 105°, as for the system at 370 pm. The curve is included in Figure 8.

The Isoelectronic Analogy to HCCH²⁺. To enhance our understanding of the bonding and bending in HTI-TIH, it is perhaps worthwhile to draw an analogy with the "isoelectronic" HCCH²⁺ and HHeHeH²⁺. We showed that s,p mixing is highly relevant for a bonding interaction in HTI-TIH. Of course, in the acetylene dication one would not doubt for a moment the necessity of s,p hybridization, nor the presence of a C-C bond (C-C overlap population: +1.42). On the other hand, we think it is unlikely anyone would argue for the existence of the HHeHeH dianion, since no unfilled orbitals are readily available to change the repulsion in this all-filled system into an attraction (He-He/H-He overlap populations: -0.35/-0.95). So low-lying p orbitals are required for bonding, but what do they have to do with bending, nonlinearity of the HEEH molecule?

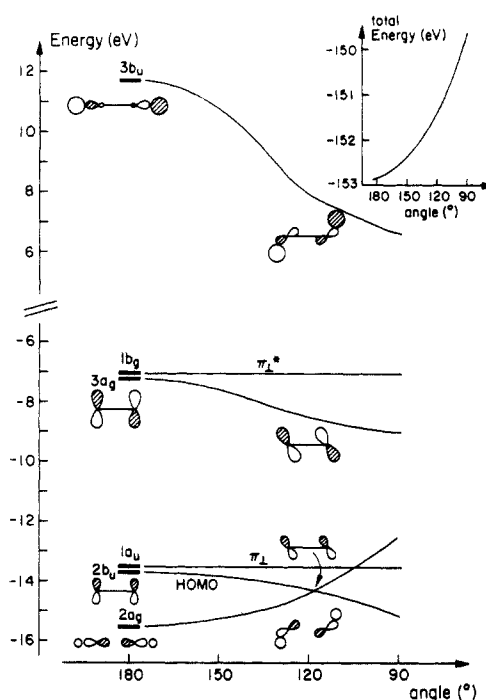


Figure 11. Partial Walsh diagram for the bending in HCCH²⁺, with C-C = 120 pm, C-H = 105 pm. The insert shows the total energy as a function of the bending angle. Symmetry labels are for C_{2v}; orbital sketches are schematic. π_⊥, π_⊥*: π sets perpendicular to the plane of the molecule.

In answering the question why HTI-TIH is bent, the acetylene analogy proves helpful, after a look at its Walsh diagram in Figure 11. The close C-C contact and the concentrated C orbitals push the C-C σ* combination (3b_u) up to very high energy, so that its mixing with the 2b_u HOMO becomes very small. Upon bending the 2a_g HOMO-1 is raised more in energy than the 2b_u is lowered—the system gets destabilized and the C-C overlap population decreases. Thus, the large 2b_u-3b_u energy separation in HCCH²⁺ prevents bending. In HTI-TIH, however, the M-M contacts are larger and the TI orbitals more diffuse. Therefore, 2b_u and 3b_u come closer in energy and their resonance gives a strong driving force for bending.

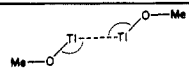
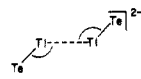
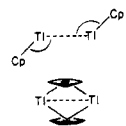
The tendency for trans-bending in H₂GeGeH₂ or H₂SnSnH₂ (6) with respect to ethylene, H₂CCH₂, can be explained by the same one-electron MO treatment, as shown in recent studies on the stabilizing mixing of σ with π* and π with σ* orbitals during the trans-bending of a double bond in R₂X=XR₂ systems.¹²⁰ The trans-bent distortion of such a double bond was traced to the singlet-triplet separation in divalent R₂X: being larger than a quarter of the total X=X (σ + π) bond energy.

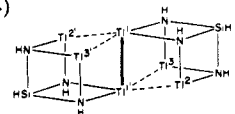
Ligands Other than Hydrogen in TI-TI Systems. In Table IV, the overlap populations for some "more realistic" systems, with ligands other than hydrogen, are given. One notices that the trend with a maximum at 120° and a considerably smaller, or even antibonding, overlap population in the linear (180° angle) and rhombic case (bridged situation) seems to be general, even though individual numbers may vary. We attribute the significantly smaller variation in overlap population in the case of the methoxy ligands to the more ionic TI-O bond, which originates from the orbital energy differences (different electronegativities) and the long bond length. An ionic bond results in a TI-TI moiety being more like TI₂²⁺, so that some overlap population is retained even for the bridging geometry. Shortening of the TI-O bond to a

(120) (a) Malrieu, J.-P.; Trinquier, G. *J. Am. Chem. Soc.* **1989**, *111*, 5916. (b) Trinquier, G.; Malrieu, J.-P. *J. Am. Chem. Soc.* **1987**, *109*, 5303. (c) Liang, C.; Allen, L. C. *J. Am. Chem. Soc.* **1990**, *112*, 1039. (d) See also the important analysis of double bonded vs bridged structures: Trinquier, G. *J. Am. Chem. Soc.* **1990**, *112*, 2130.

(121) (a) Burdett, J. K. *Inorg. Chem.* **1981**, *20*, 1959. (b) Pearson, R. G. *J. Am. Chem. Soc.* **1969**, *91*, 4947. (c) Öpik, U.; Pryce, M. H. L. *Proc. R. Soc.* **1957**, *A238*, 425.

Table IV. Overlap Population as a Function of the Ligand and Angle in Tl^I-Tl^I Systems with $d(\text{Tl-Tl}) = 370 \text{ pm}^a$

system	angle, deg L-Tl-Tl	overlap pop (total)
(1) 	180 (linear)	0.242
	120	0.353
	45 (rhombus)	0.118
(2) 	180 (linear)	0.045
	120	0.411
	51 (rhombus)	-0.012
(3) 	180 (linear)	0.177
	131.8 (exp)	0.347
	120	0.367
	42 (rhombus)	-0.044

(4) 	contact	dist, pm	overlap pop
	Tl ^I -Tl ^{I'}	315	0.468
	Tl ^{I'} -Tl ^{2,3}	368	0.236
	Tl ^I -Tl ^{2',3'}	368	0.236
	Tl ^I -Tl ^{2,3}	393	0.029
	Tl ^{I'} -Tl ^{2',3'}	393	0.029

^aTl-ligand bond distances were chosen according to experimental parameters: (1) cf. ref. 5; Me = methyl, Tl-O = 261.6 pm, Tl-O-Me = 120° (135° at L-Tl-Tl = 45°), O-C = 143 pm, C-H = 110 pm. ^bCf. ref 6; Tl-Te = 295 pm. ^cCf. ref 25; Cp = cyclopentadienyl, Tl-Cp(centroid) = 249 pm, centroid-C = 121.64 pm, C-C = 143 pm, C-H = 108 pm, exp = experimental value for $\{(\text{PhCH}_2)_5\text{C}_5\text{Tl}\}_2$ (3). ^dCf. ref 30 and 31; the model molecule drawing is rather schematic; Tl^I-N = 237; Tl^{2,3,2',3'}-N = 249; N-Si ≈ 175; N-H = 100; Si-H = 148; Si-Tl ≈ 315 pm.

covalent 212 pm (sum of the covalent radii) gives a smaller overlap population at 180° (0.120), a larger maximum (0.426), and a small antibonding overlap population for the rhombic case (-0.013). We wonder if the small bonding overlap population still found for the bridged dithallium methoxide species could be correlated to the weak Tl...Tl bonds of the tetrameric alkoxides, postulated from an analysis of their vibrational spectra.¹³

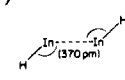
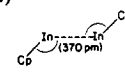
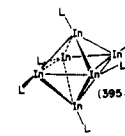
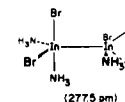
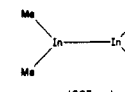
Also included in Table IV is a brief overlap population description of a model for the $\{\text{MeSi}(\text{N}^i\text{Bu})_3\text{Tl}\}_2$ complex with one amazingly short Tl-Tl contact of 315.2 pm.^{30,31}

In^I-In^I Interactions. One does not expect and indeed does not see any fundamental changes in the interaction between two In^I...In^I centers when compared to thallium at the same separation. Of course, the indium-indium interaction at the same distances and angles will be smaller than the one observed for thallium, due to the smaller size of the indium atom. Table V gives the overlap populations for three indium systems at different angles. To get an idea of the value of the overlap population for the "realistic" In-In bond in $\text{In}_2\text{Br}_4 \cdot 2\text{men}^{44}$ and $\{[(\text{Me}_3\text{Si})_2\text{CH}]_2\text{In}^{\text{II}}\}_2$,⁴⁵ we calculated the model complexes $\text{In}_2\text{Br}_4 \cdot 2\text{NH}_3$ and Me_4In_2 with distances and angles adapted from the real structures. These values are included in Table V. The larger overlap populations are, of course, expected for the shorter In-In distances. But they may also be attributed to the nonfilling of In-In antibonding levels, due to the +II oxidation state.

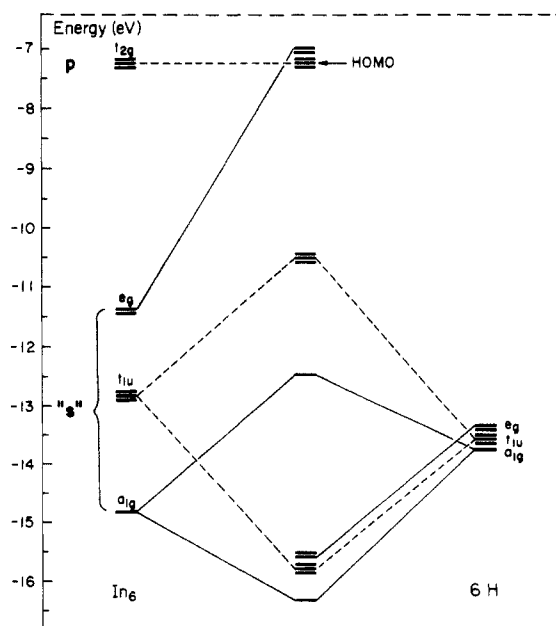
While the variation and magnitude of the overlap population for HIn-InH and $(\text{H}_3\text{C})_3\text{In-In}(\text{C}_5\text{H}_5)$ is as expected at 370 pm In-In separation, the large overlap population for In_6H_6 came as a surprise, considering the long In-In distance of almost 400 pm.

The In hexamer cluster is worth a closer look. For L = H there is quite a large overlap population at an $O_h(\text{centroid})\text{-In-H}$ angle of 180°. The overlap population decreases slowly upon bending the hydrogen toward an octahedral face to give an S_6 -symmetry molecule (see Table V). A simplified molecular orbital diagram given in Figure 12 demonstrates the reason for the large In-In overlap population. The filled orbitals of the In_6^{6+} and the H_6^{6-} fragments form sets of a_{1g} , t_{1u} , and e_g symmetry. Their interaction gives rise to the formation of an In-H bonding, $a_{1g} + t_{1u} + e_g$ set (mainly H in character) and an In-H antibonding $a_{1g}^* + t_{1u}^* + e_g^*$ combination (mainly In based). The mixing in from higher

Table V. Overlap Populations in In^I-In^I Systems

system ^a (d(In-In))	angle, deg	overlap pop (total)
(1) 	L-Tl-Tl	
	180	-0.185
	150	0.207
	120	0.303
	90	0.284
(2) 	180	-0.040
	136.5 (exp)	0.168
	120	0.212
	90	0.172
(3) 	L-In-O _h (centroid)	
	L = H	
	180	0.236
	150	0.147/0.152
	120	0.128/0.133
	L = Cp	
	180	0.030
147.5 (exp)	0.085/0.083	
140	0.090/0.086	
120	0.073/0.072	
(4) 	In ^{II} -In ^{II}	0.828
		0.804

^a(1) In-H = 175 pm, estimated from the sum of the covalent radius of In (139 pm)⁴⁴ and H (37 pm). (2) Cf. ref 42; Cp = cyclopentadienyl, In-Cp(centroid) = 238.2 pm, centroid-C = 121.64 pm, C-C = 143 pm, C-H = 108 pm, exp = experimental value for $\{(\text{PhCH}_2)_5\text{C}_5\text{In}\}_2$ (3). (3) Cf. ref 41; In-H = 175 pm, regular octahedral In_6 cluster; Cp = cyclopentadienyl, In-Cp(centroid) = 230 pm, centroid-C = 119.857 pm, C-C = 140.9 pm, C-H = 100 pm, exp = experimental value for $\{\text{Me}_5\text{C}_5\text{In}\}_6$. (4) $\text{In}_2\text{Br}_4 \cdot 2\text{NH}_3$; cf. ref 44; distorted trigonal-bipyramidal ligand coordination around indiums with the equatorial planes of each trigonal bipyramid perpendicular to each other; In-Br = 270 pm, In-N = 240 pm, N-H = 100 pm, In-In-Br_{eq}/N_{eq} = 128°, In-In-Br_{ax} = 92°, In-In-N_{ax} = 95°, In-N-H = 110°. In_2Me_4 ; cf. ref 45; Me = methyl, In-C = 219 pm, C-H = 110 pm, In-In-C = 120°, planar molecule.

**Figure 12.** Partial, simplified MO diagram for the In_6H_6 octahedral cluster, with $O_h(\text{centroid})\text{-In-H} = 180^\circ$, In-In = 395, In-H = 175 pm.

lying empty In orbitals of the appropriate symmetry is not shown in Figure 12. The In-In antibonding e_g^* orbital is pushed above the empty, partly In-In bonding, 3-fold degenerate t_{2g} orbital in energy. This explains the large overlap population—initially unexpected at this In-In separation of almost 400 pm. The near degeneracy of the t_{2g} and e_g^* provides an obvious opportunity for a second-order Jahn-Teller effect^{110,121} to work. In S_6 t_{2g} splits into $e_g + a_g$, while e_g^* remains degenerate. The two e_g sets interact strongly, stabilizing the molecule along the deformation coordinate. The molecule of S_6 symmetry (7) obtained upon hydrogen bending is expected to have two sets of In-In bonds of unequal strength: one for the In_3 triangles around the S_6 axis (here found to be weaker) and one between these triangular units (stronger). We note that the X-ray structure of the parent pentamethylcyclopentadienylium hexamer⁴¹ also shows two sets of slightly different In-In distances in the S_6 symmetry molecule, with the In-In separations in the triangles around the S_6 axis being slightly larger (396.3 pm) than in between them (394.2 pm). The observed trend is small but matches the pattern of the overlap population values.

We also calculated a more realistic cyclopentadienylium hexamer, $\{C_5H_5In\}_6$, for comparison. In the high-symmetry conformer, at an O_h (centroid)-In-Cp(centroid) angle of 180° , one obtains equal In-In overlap populations of 0.030. The small overlap population follows from a $(e_g^*)^4(t_{2g})^0$ configuration, i.e. the e_g^* level now is below the t_{2g} . Bending the Cp ligands over an In_3 face (7) increases the In-In overlap population to a maximum of 0.090/0.086 at an angle of 140° . The anticipated, two very slightly different sets of overlap populations again correlate with the slightly different observed In-In "bond" lengths in the pentamethylcyclopentadienyl parent cluster. The energy minimum for the bending in $\{C_5H_5In\}_6$ also occurs at an angle of 140° . The observed O_h (centroid)-In-Cp*(centroid) bending angle in $\{Me_5C_5In\}_6$ is 147.5° (calculated by us from the atomic coordinates⁴¹).

Do these rather small overlap populations imply the existence of In...In interactions? Certainly some bonding is present, even if it is not large.

We could expect the bonding to be much stronger if the hexamer is partially oxidized, i.e. if the six, mainly In s combinations were filled with less than 12 electrons. Such a situation can be found in the hexameric clusters of late transition metals with formally closed d^{10} and partially filled s levels. Examples are $[Au_6(P(p-C_6H_4CH_3)_3)_6]^{2+}$, $[BPh_4]^{2-}$,¹²² $Zn_4Ni_2(C_5H_5)_6$, and $Zn_4Ni_2(C_5H_5)_4(C_5Me_5)_2$,¹²³ which contain formally two electrons in the s levels. A d-s-p mixing will, of course, be important as well for the bonding in these transition-metal octahedral clusters.

The Solid State

To analyze the bonding relationships in extended systems of formally closed subshell Tl^+ or In^+ centers, we will investigate two model systems, a chain and a two-dimensional square net. Both geometrical features are found in the majority of Tl or In solid-state complexes (see Table II). Looking at undistorted linear chain or net arrangements, we will then consider the effect of electronic perturbations, specifically the influence of counterions surrounding each Tl/In in a chain or net in different geometries. The electronic structure in the specific cases of Tl and In monohalides has also been analyzed elsewhere.¹¹⁸

We will start, however, with a brief study of the effect on the bonding in a $Tl-Tl^{2+}$ pair if each Tl is brought into an octahedral or cubic crystal field of negative ions. This approach serves to model Tl_2^{2+} pairs in a solid-state complex, but more importantly it will give us within a molecular model a first idea of the effects we will encounter in the extended structures.

(122) Bellon, P.; Manassero, M.; Sansoni, M. *J. Chem. Soc. Dalton* **1973**, 2423. See also: Briant, C. E.; Hall, K. P.; Mingos, D. M. P. *J. Organomet. Chem.* **1983**, 254, C18.

(123) (a) Budzelaar, P. H. M.; Boersma, J.; van der Kerk, G. J. M.; Spek, A. L.; Duisenberg, A. J. M. *Organometallics* **1985**, *4*, 680. (b) Fischer, B.; Kleijn, H.; Boersma, J.; van Knoten, G.; Spek, A. L. *Organometallics* **1989**, *8*, 920.

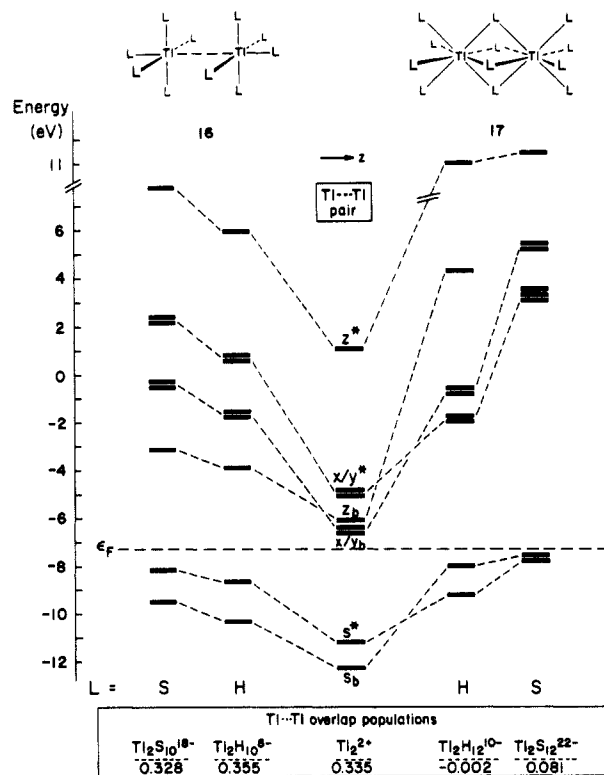
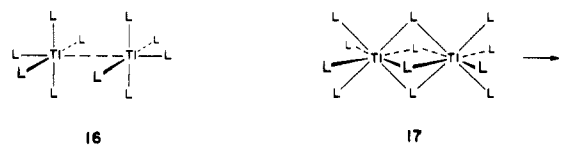


Figure 13. Ligand field effects with a square-pyramidal and cubic coordination of hydrogens or sulfurs on a Tl_2 pair. $Tl-Tl = 370$ pm, $Tl-H = 267$ pm, $Tl-S = 324$ pm.

The interaction between two adjacent indium cyclopentadienyl chains, which gives rise to the formation of In pairs, will be examined. For the sake of comparison, the $Tl...Tl$ separation in the Tl_2^{2+} pairs and Tl_∞ chains will be kept at 370 pm throughout our calculations, unless indicated otherwise.

A description of the theoretical and analytical tools for understanding extended structures may be found in a recent book.¹¹¹ The density of states (DOS) we will use in our calculations measures the number of a given type of orbital (here only atomic orbitals) per unit volume and unit energy. In the DOS curve, the energy as ordinate is plotted versus the DOS as abscissa. An integration of the DOS over a certain energy interval gives the number of orbitals (per unit volume and energy interval), normalized and expressed as a percentage of the total DOS (see for example Figure 14). Bond strengths in the solid state are measured by the crystal orbital overlap population (COOP). The COOP curve is obtained by weighting the DOS in each energy interval by its contribution to the overlap population (see for example Figure 14).

The Ligand Field Effect on Tl_2^{2+}/In_2^{2+} . We choose to look at Tl_2^{2+} pairs, where each Tl is coordinated by the ligand in either a square pyramidal (16) or cubic (square prismatic 17) way.



Distorted examples of the first coordination mode are found in $Tl_2As_2S_4$,⁵² Tl_3Se_2I ,⁵³ and $In_6La_{10}O_6S_{17}$,⁵⁹ for the second one in Tl_2SnSe_3 .⁵⁴ Hydrogen and sulfur were chosen as ligands for our model systems. The $Tl-S$ distance was fixed at the sum of the crystal of ionic radii (Tl^+ , 140 pm;^{124a,125} S^{2-} , 184 pm^{124b,125,126}).

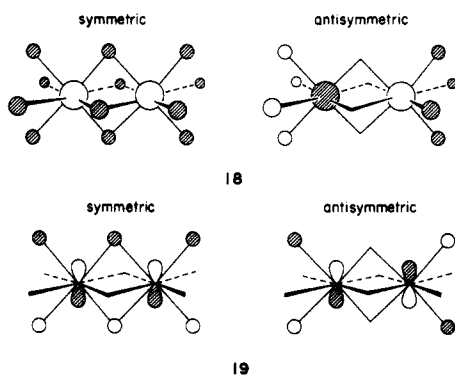
(124) (a) Pauling, L. *The Nature of the Chemical Bond*, 3rd ed.; Cornell University Press: Ithaca, NY, 1963; Table 13.5, p 518. (b) *Ibid.* Table 13.3, p 514. See also Pauling, L. *The Chemical Bond*; Cornell University Press: Ithaca, NY, 1960; Table 7.8, p 151.

(125) Ball, M. C.; Norbury, A. H. *Physical Data for Inorganic Chemists*; Longman: London, 1974.

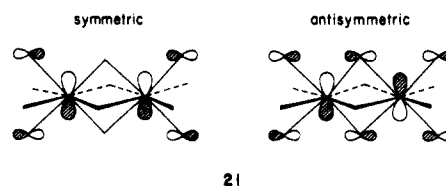
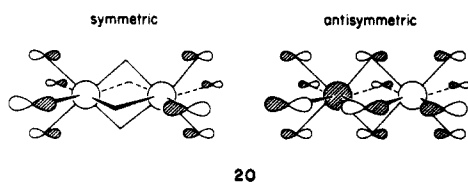
Although the hydrogen ligand behaves like a hydride (H⁻) ion, the Tl-H separation was taken as 267 pm from the sum of Tl⁺ 140 pm and H⁺ 127 pm.¹²⁶ This turned out to be a reasonable estimate, judging from the similarity of the results for the thallium hydride and thallium sulfide calculations. Each H ligand was assigned a -1 charge and each S a -2 charge to give Tl₂H₁₀⁸⁻, Tl₂S₁₀¹⁸⁻, Tl₂H₁₂¹⁰⁻, and Tl₂S₁₂²²⁻ model complexes. As could be anticipated, the main ligand field effect consists of raising the thallium levels in energy relative to an isolated Tl₂ pair, as shown in Figure 13. With a square-pyramidal coordination sphere (16), the degenerate x/y levels are of course raised the most, since four ligands point directly toward them. However, the square-pyramidal environment does not affect the s-z mixing, thus leaving the Tl...Tl overlap population basically unchanged.

This is quite different from the result seen in a square-prismatic (cubic) environment (17). Again, the levels are raised with respect to an isolated Tl₂ pair, but also the overlap population is decreased considerably. This can be traced to a virtual elimination of z mixing into the Tl s levels, because the z orbitals are pushed up so much higher in energy than the s orbitals. Therefore, their relative energy difference, to which the mixing is inversely proportional, increases from about 12.3 eV for the important z*-s* energy difference in an isolated Tl₂ pair to over 18 eV in a square-prismatic field. At the same time the cubic coordination sphere pushes the Tl levels, which are symmetric with respect to the mirror plane along the shared prism face, up to higher energy than the antisymmetric orbitals. Except for the z orbitals, bonding orbitals lie then at higher energy than antibonding ones. Because of the vertical mirror plane in-between the two thalliums, s orbitals on the ligands within this mirror plane can contribute only the destabilizing crystal field for those Tl orbitals that are symmetric with respect to this plane (which happen to be Tl-Tl bonding combinations). The reversal of the natural energy ranking, bonding below antibonding, is due to a through-bond coupling effect, which has been analyzed in detail by one of us in molecular¹²⁷ and extended¹²⁸ edge-sharing tetrahedra. Long metal-metal distances create the opportunity for through-bond effects to operate.

The actual ligand s orbital combinations for the Tl s and x levels in Tl₂H₁₂¹⁰⁻ are sketched in 18 and 19, to help us visualize what has just been said.



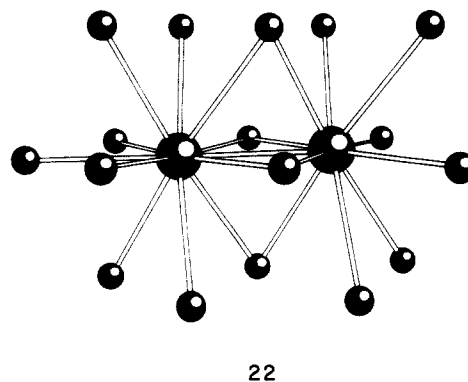
The reverse is, of course, true for the ligand p orbitals (on sulfur), but due to their more diffuse nature, they exert a weaker ligand field. Ligand p orbital combinations with Tl s and x levels are drawn in 20 and 21.



The p level on sulfur, however, account for the difference in the energy diagram of Tl₂H₁₂¹⁰⁻ and Tl₂S₁₂²²⁻. They are responsible for raising the x/y orbitals to even higher energies, as a result of interactions of type 21. The partial reversal in the ligand field strength on the symmetric and antisymmetric Tl s MO's, comparing ligand s and p orbitals (18 vs 20), leads to the close energy of the Tl s and s* levels for Tl₂S₁₂²²⁻.

The reason for this rather elaborate discussion of the Tl₂ pairs will become apparent when we discuss the infinite Tl chains. There, we will also look at the square planar (cf. square pyramidal) and cubic ligand field. The splitting of the crystal orbitals in the infinite chain, i.e. the dispersion of the bands, can be explained with the same picture we just developed. Tl₂X₁₂ⁿ⁻, especially, is a segment of such a chain and its orbitals can be viewed as a miniband.

In the cluster Tl_{0.8}Sn_{0.6}Mo₇O₁₁, we also have a Tl₂ pair (with a very short distance of 284 pm), although here Tl is in the +II oxidation state, based on an Tl-O distance analysis.⁹⁵ To get an idea on the overlap population of a genuine Tl-Tl single bond⁹⁵ (cf. In^{II} complexes in Table V), we calculated the Tl pair with its immediate oxygen coordination sphere (Tl₂^{II}O₁₇³⁰⁻) as a model to compare with the values from our calculations of 16 and 17 (Figure 13). The rather complicated, irregular anion environment composed of 17 oxygens (with Tl-O ranging from 262.0 to 304.8 pm) may be evident from 22. While 12 oxygens are positioned in a distorted face-sharing cubic fashion as in 17, the five re-



maining ones correspond to part of the square-pyramidal arrangement in 16 with four at an approximately 90° angle with respect to the Tl-Tl bond (two at each Tl) and one in the axial position (~180° angle).

In light of this ligand geometry, predominantly as in 17, it is not surprising that our calculations give a smaller Tl^{II}-Tl^{II} overlap population (0.478) than for a bare Tl^{II}-Tl^{II} pair (0.54) at this distance. At such a short separation we find, of course, the "natural" orbital energy ordering of bonding below antibonding orbitals, as opposed to the through-bond coupling pattern in 17 (Figure 13). The Tl-Tl overlap population of 0.478 for Tl₂^{II}O₁₇³⁰⁻, 22, compares favorably with the values we calculated for the square-pyramidal ligand geometries in the dimers (16, Figure 13) and the values we will see later on for the square-planar-coordinated chains (Table VIII). In view of all these overlap populations being not too different, we feel confident of assigning similar bond strengths and orders to the Tl-Tl interactions in these compounds.

Before proceeding, however, to the infinite Tl⁺ chains, we will look at a specific example of In-In²⁺ pairs. An X-ray crystal structure investigation of (C₅H₅)In and (MeC₅H₄)In revealed parallel, polymeric $\cdot\text{In}\cdots\text{Cp}\cdots\text{In}\cdots\text{Cp}\cdots$ (Cp = C₅H₅ or MeC₅H₄) zigzag chains with In \cdots In interchain distances of 398.6 pm in both

(126) Wyckoff, R. W. G. *Crystal Structures*, 2nd ed.; Interscience Publishers: New York, 1968; Vol. 4, Table XIII.6, p 524.

(127) Summerville, R. H.; Hoffmann, R. J. *Am. Chem. Soc.* **1976**, *98*, 7240.

(128) Silvestre, J.; Hoffmann, R. *Inorg. Chem.* **1985**, *24*, 4108.

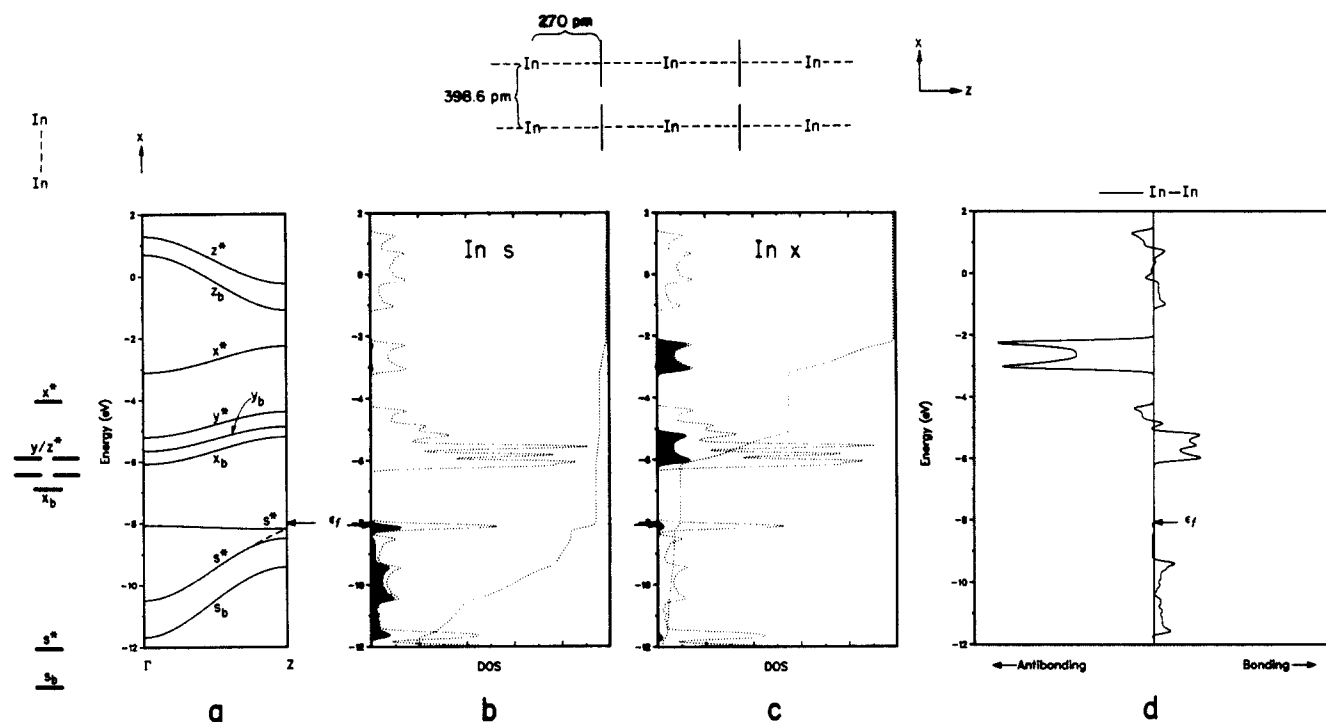
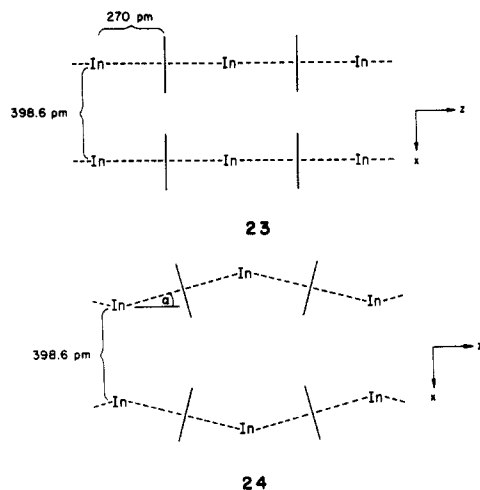


Figure 14. (a) Band structure diagram of the indium bands in the linear CpIn double chain (**23**) with the energy levels of an isolated In...In dimer at the left-hand side. (b, c) Density of state (DOS) plots for selected In orbitals in **23** (shaded area) with integration and total DOS (dotted lines). (d) Projected overlap population (COOP) between the indiums in **23** (average 0.160). A 30K-point set was used for the average property (DOS, COOP) calculations; C-C = 136, C-H = 100 pm; cf. ref 43.

cases. In $\{(\text{MeC}_5\text{H}_4\text{In})_\infty\}$ each In is in contact with one other In, while in $\{(\text{C}_5\text{H}_5\text{In})_\infty\}$ each In has two other In neighbors.^{26,43} Although the bonding in a polymeric $\text{C}_5\text{H}_5\text{M}$ (M = In, Tl) chain has already been analyzed,¹²⁹ possible interchain interactions have not been looked at. For our purpose, we constructed two parallel $\{(\text{C}_5\text{H}_5\text{In})_\infty\}$ chains, closely based on the experimental, structural parameters.⁴³ Starting from a linear geometry (**23**), we went to a zigzag chain (**24**) with different bending angles α .



The undistorted double chain can also be viewed as a stacking of In...In²⁺ dimers insulated by cyclopentadienyl anions, which surround each In in a linear fashion. Each molecular orbital of the In...In dimer is spread into a band in the InCp double chain. The degeneracy of the y/z orbitals in the dimer is of course broken up in the chain. The center of each crystal orbital or band is then pushed up with respect to the molecular orbitals of the dimer. This is due to the ligand field of the Cp rings. The z combinations, which are pointed directly toward the rings, experience, of course,

Table VI. In-In Overlap Populations as a Function of the Bending Angle in InCp Double Chains^a

	bending angle, deg		In-In overlap pop ^c
	α^b	Cp-In-Cp	
0		180	0.160
10		160	0.146
20		140	0.146
25		130 (exp)	0.136
unligated dimer			0.094

^a A 10K point set was used in the calculations, In-In = 398.6 pm, In-Cp(centroid) = 270 pm as indicated in **23** and **24**; centroid-C = 115.69 pm, C-C = 136 pm, C-H = 100 pm; cf. ref 43; exp = approximate experimental value for $\{(\text{C}_5\text{H}_5\text{In})_\infty\}$ and $\{(\text{MeC}_5\text{H}_4\text{In})_\infty\}$.⁴³ ^b For a definition of the bending angle α see **24**. ^c The values refer to the In-In pair whose distance remains unchanged at 398.6 pm upon bending.

the strongest field and are pushed up the most. Figure 14a displays the bands of the InCp double chain, which are predominantly In in character, together with the orbital energy levels of the molecular In dimer. In addition to the eight expected In bands, a ninth (very flat) band right at the Fermi level is shown. This valence band acquires substantial In character when going from Γ to Z, due to an avoided crossing with the In band right underneath it. This can be followed from the projected DOS of the In s orbitals in Figure 14b.

Although the In...In separation of almost 400 pm is rather long, still a fairly large overlap population, larger even than in the unligated In...In dimer, is found (Table VI). This can be explained from the projected DOS of the In x orbitals in Figure 14c and the COOP plot in Figure 14d. Unlike the HOMO in the In₂²⁺ dimer, which is antibonding in character (overlap population -0.067, cf. the interaction diagram for the Ti₂²⁺ dimer in Figure 2), the filled In bands in the chain are only bonding and non-bonding, as seen from the COOP plot in Figure 14d. The non-bonding feature of the highest filled In band is due to an increased mixing in of x character, especially at its top (note the little peak at -8 eV in the projected x orbital density of states plot in Figure 14c) to relieve the antibonding s-s overlap. From the integration in Figure 14c it can be seen that altogether 10% of the In x orbitals contribute to the filled levels, compared to about 5% in the In-In

(129) (a) Canadell, E.; Eisenstein, O.; Rubio, J. *Organometallics* **1984**, *3*, 759. (b) We also refer to some unpublished work by D. Gilbert on polymeric indium phospholes, Cornell University, 1989.

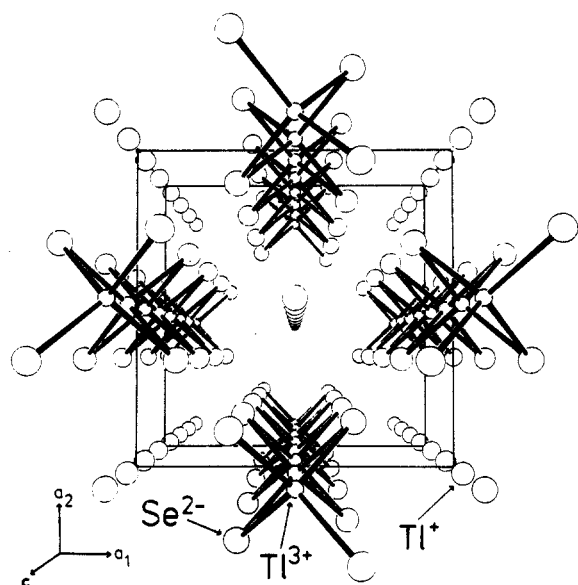


Figure 15. Perspective view of the TlSe-type structure along *c*. Reprinted with permission from ref 64. Copyright 1985 Buchexport, Leipzig.

dimer. This enhanced *s*-*x* mixing can occur through the cyclopentadienyl orbitals of the conduction band.

Upon kinking the InCp double chain according to **24**, the overlap population of every second In...In pair is only slightly decreased as one moves toward the approximate experimental Cp(centroid)-In-Cp(centroid) angle of 130° (128.02° for $\{(C_5H_5)In\}_\infty$, 130.66° for $\{(MeC_5H_4)In\}_\infty$)⁴³ (see Table VI).

Linear Thallium and Indium Chains. Perfectly linear and equidistant Tl⁺ (and In⁺) chains are found for example in structures of the TlSe type⁶⁰⁻⁶⁴ (see Figure 15) in TlCu₇S₄,⁷⁰ TlCu₇Se₄,⁷¹ and Tl₂SnO₃,⁹¹ as part of a larger framework. The Tl...Tl intrachain distances range from the arbitrarily imposed limit of nearly 400 pm in TlCu₇Se₄ to 323 pm in Tl₂SnO₃. One finds In...In intrachain distances as short as 286 pm in InMo₄O₆.⁷⁵ The complexes that contain linear In⁺ chains with remarkably short In...In separations, namely InGaSe₂ (315.8 pm)⁶⁴ and InMo₄O₆ (286.3 pm),⁷⁵ were also reported to be highly conducting, metallic along the chain direction ($\sim 10^4 \Omega^{-1} \text{cm}^{-1}$ at *T* = 293 K, and $0.63 \times 10^4 \Omega^{-1} \text{cm}^{-1}$ at *T* = 298 K, respectively).

Let us consider a simple linear Tl chain, with no ligands at first. The band structure for a linear Tl chain with one Tl atom per unit cell is shown in Figure 16. The crystal orbitals are illustrated at the special points Γ and Z. At Γ the unit cells are all in-phase, while at Z they are all out-of-phase to each other. The *s* and *x/y* crystal orbital combinations are most bonding and therefore of lowest energy at Γ and most antibonding or of highest energy at Z. The bands are said to "run up" from Γ to Z.¹¹¹ On the contrary, the *z* band is most antibonding (highest energy) at Γ , with the *z* orbitals being all in phase, and most bonding (lowest energy) at Z, with neighboring orbitals being out-of-phase. Hence, it "runs down". At the special points, the zone center Γ and zone edge Z, all bands are purely *s*, *x/y*, or *z*, respectively, in character. However, since the *s* and *z* band have the same symmetry, they can mix throughout the Brillouin zone, i.e. between Γ and Z, much like the *s*-*z* mixing in the Tl-Tl dimer. This mixing can be followed from the DOS projections in Figure 17, which show from the integrations that about 12% *s* character is distributed throughout the *z* band (Figure 17a), while the same amount of *z* contribution mixes into the *s* band (Figure 17b). The *x/y* band remains of course localized (Figure 17c). The band structure shown together with the DOS plots should demonstrate the relationship between both. We would like to note that the *s* and *z* band do not exhibit an avoided crossing down to a Tl...Tl separation of 320 pm.

Concerning the perfect linearity of the Tl/In chains, in a Tl¹⁺ or In¹⁺ chain, the lowest band (in Figure 16) would be completely filled by the two *s* electrons. Hence, in a first approximation, there

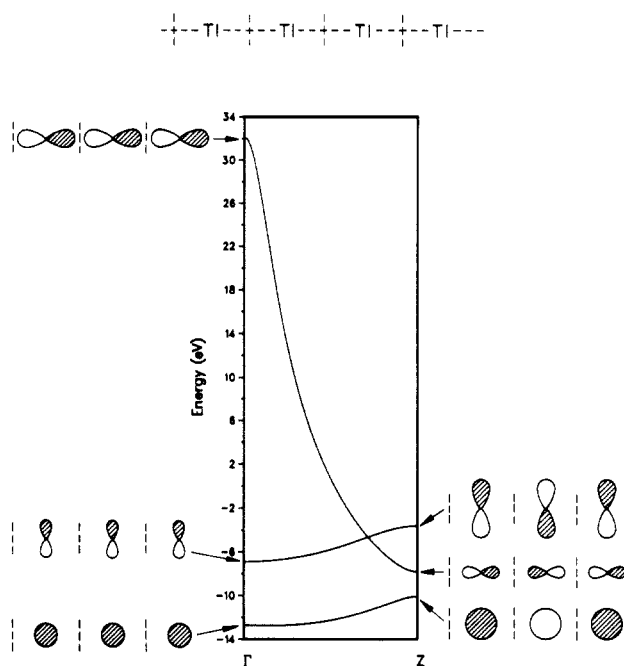


Figure 16. Band structure diagram of a linear Tl chain (Tl-Tl = 370 pm) with one Tl per unit cell, and schematic orbital representations at the zone center and edge (special *k* points Γ and Z). For the degenerate π set, only one representative is drawn out. Dashed, vertical lines indicate unit cell boundaries.

Table VII. Tl...Tl/In...In Overlap Populations as a Function of Distance in One-Dimensional Linear Chains^a

distance, ppm	overlap population ^b	
	Tl...Tl	In...In
370	0.289	
350	0.370	0.253
340	0.417	
320	0.538	0.516
290		0.691
270		0.775

^a Unligated metal chains; a 100K point set was used in the calculations. ^b Overlap population values are for $\{Tl^+\}_\infty$ and $\{In^+\}_\infty$ chains.

would be no incentive for a distortion. However, if one would imagine a partial oxidation of the chain, giving rise to an incompletely filled *s* band, a Peierls distortion¹³⁰ (the solid-state analogue of the Jahn-Teller effect) would be expected to occur. Such a periodic lattice distortion opens up a band gap at the Fermi level by lowering the filled and raising the empty band part in energy. This may lead to charge density waves. The occurrence of distinct In₅⁷⁺ [$=In^{2+}(In^+)_3-In^{2+}$] and In₆⁸⁺ [$=In^{2+}(In^+)_4-In^{2+}$] fragments, alternating along a chain in In₁₁Mo₄₀O₆₂,⁵⁷ could be explained as arising from such oxidation and consequent distortion.

Some numbers to illustrate the variation of Tl...Tl and In...In overlap populations with distance are given in Table VII. At the same distance (e.g. 370 pm) the overlap population value for an infinite Tl¹⁺ chain (0.289, Table VII) is smaller than that for the Tl₂²⁺ dimer (0.335, Figure 2). This can be rationalized from the DOS projection in Figure 17b. The top of the *z* band (corresponding to *z*^{*}, 2 σ_u^* in the dimer) is pushed to rather high energies (~ 32 eV, versus 1 eV in the dimer), so its important mixing into the top of the *s* band (*s*^{*}, 1 σ_u^*), to relieve its antibonding character, is greatly diminished. As can be clearly seen from the *z* projection in Figure 17b, the *z* band mainly mixes into the bottom part of the *s* band (more so than in the dimer, because they are closer in energy), enhancing its bonding character. Toward the top of

(130) (a) Peierls, R. E. *Quantum Theory of Solids*; Oxford University Press: London, 1955; p 108. (b) Whangbo, M.-H. *Crystal Chemistry and Properties of Materials with Quasi-One Dimensional Structures*; Rouxel, J., Ed.; D. Reidel: Dordrecht, The Netherlands, 1986; p 27.

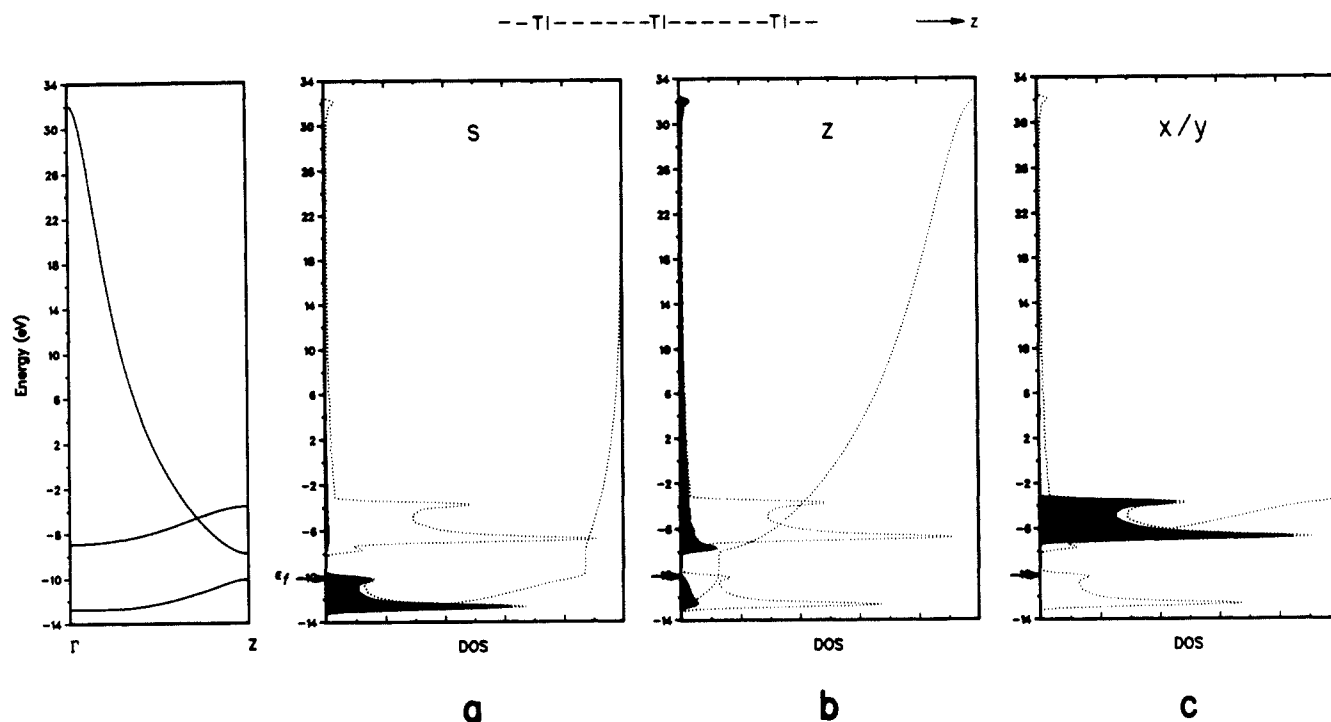


Figure 17. Density of state (DOS) projections for the three different kinds of orbitals in a linear Tl chain (Tl-Tl = 370 pm): s (a), z (b), and x/y orbital (π set) (c), shaded areas, with integrations and total DOS (dotted lines). The Fermi level indication is for $\{\text{Tl}^+\}_\infty$. The band structure diagram from Figure 16 is repeated at the left-hand site to demonstrate the relationship between these representations. (Note: DOS and COOP plots are independent of the number of atoms per unit cell.)

the s band, the z contribution falls off sharply.

Now we study the changes in the band structure if each Tl in the chain experiences a ligand field. We again choose hydrogen and sulfur as model ligands with Tl-L distances as assumed above for the related $\text{Tl}_2^{2+}/\text{In}_2^{2+}$ discrete molecular models. The ligand geometries observed for the linear metal chains are the square antiprism for the TlSe-type structures,⁶⁰⁻⁶⁴ the cube or pseudocubic prism for TlCu_7Se_4 ,⁷¹ respectively TlCu_7S_4 ,⁷⁰ and a square-planar coordination in InMo_4O_6 .⁷⁵ Also, the In_5 and In_6 chain segments in $\text{In}_{11}\text{Mo}_{40}\text{O}_{62}$ have a close to square-planar oxygen coordination for the middle indiums.⁵⁷

Generally, the Tl bands are pushed up to higher energy in a ligand field. However, as was seen in the previous section (ligand effect on Tl_2 pairs) not all bands (orbitals) are affected the same way, depending upon the ligand geometry and the ligand itself. For example, a square-planar hydrogen coordination will not have any effect on the Tl z band due to symmetry. The x/y and the s band will simply be pushed up in energy (the s band less so) without change in morphology. This can be seen from a comparison of parts a and b of Figure 18. The s and z bands in Figure 18b almost touch each other at this chosen geometry, but do not show an avoided crossing yet. On the other hand a cubic hydrogen field will not only influence the z band within the Brillouin zone and at Z (but not at Γ) but also change the slope of the x/y and s band (Figure 18c). Due to symmetry, the full interaction of the hydrogen ligands with Tl x/y and s bands occurs at Γ and no mixing takes place at Z. Therefore, the energy for the Tl-Tl antibonding crystal orbitals at Z is still the same as for the unligated chain, while the bonding crystal orbitals at Γ are pushed up higher in energy, so that the band runs down. This is identical with the reversal of the natural energy ordering for the bonding and antibonding orbitals of the molecular Tl_2 pair in a cubic field. Orbital sketches are included in Figure 18b,c to clarify the interactions. The flat bands at the bottom of the diagrams in Figure 18b,c below -12 eV are part of the hydrogen bands.

With sulfur as a ligand things are changed a little bit by the presence of additional p orbitals. As shown in Figure 18d, the Tl z band gets pushed up at Γ in a square-planar arrangement. Also included in the diagram in Figure 18d are the sulfur p bands (below -10 eV); they will be omitted for clarity from now on. In a cubic ligand field sulfur orbitals (versus hydrogen s) are available

Table VIII. Tl...Tl/In...In Overlap Populations as a Function of Ligand Field in One-Dimensional Linear Chains^a

ligand field	M	L	distance, pm		overlap pop
			M...M	M-L	
square planar 	Tl	H	370	267	0.393
	Tl	S	370	324	0.390
	In	O	290	240	0.834
cubic 	Tl	H	370	267	0.027
	Tl	S	370	324	0.075
square antiprismatic 	Tl	H	370	267	0.028
	Tl	S	370	324	0.073
	Tl	S	340	332	0.243
in 3-dimensional environment, $\text{Tl}^{\text{I}}\text{Tl}^{\text{III}}\text{S}_2$, see Figure 15	Tl	S	340	332	0.326

^a 100K point sets used in calculations, except for the full structure of TlTlS_2 , where an 18K point mesh was employed for the tetragonal unit cell.

to interact at every point in the Brillouin zone. Thus, the x/y and s bands also get pushed up at Z, although less so than at Γ . A rather flat s band results, while the slope change for x/y is still clearly visible (see Figure 18e). The overlap populations of the ligated chains are included in Table VIII. It can be seen that a square-planar ligand environment increases the overlap population, while a cubic or square antiprismatic arrangement lowers this value. In their effect on the Tl...Tl overlap population the latter two coordination modes are analogous to the bridging ligand position in the molecular Tl...Tl case. However, the origin of the effect seems to be different. While the covalently bound bridging ligand in the molecular case can be thought of as directing the sign of the s-z mixing is such a way as to have the hybrid orbitals point outside the Tl-ligand ring, the bridging ligand in the Tl chain pushes the bottom of the z band up quite high in energy. Thereby it increases the s-z energy separation (see Figure 18c,e) and

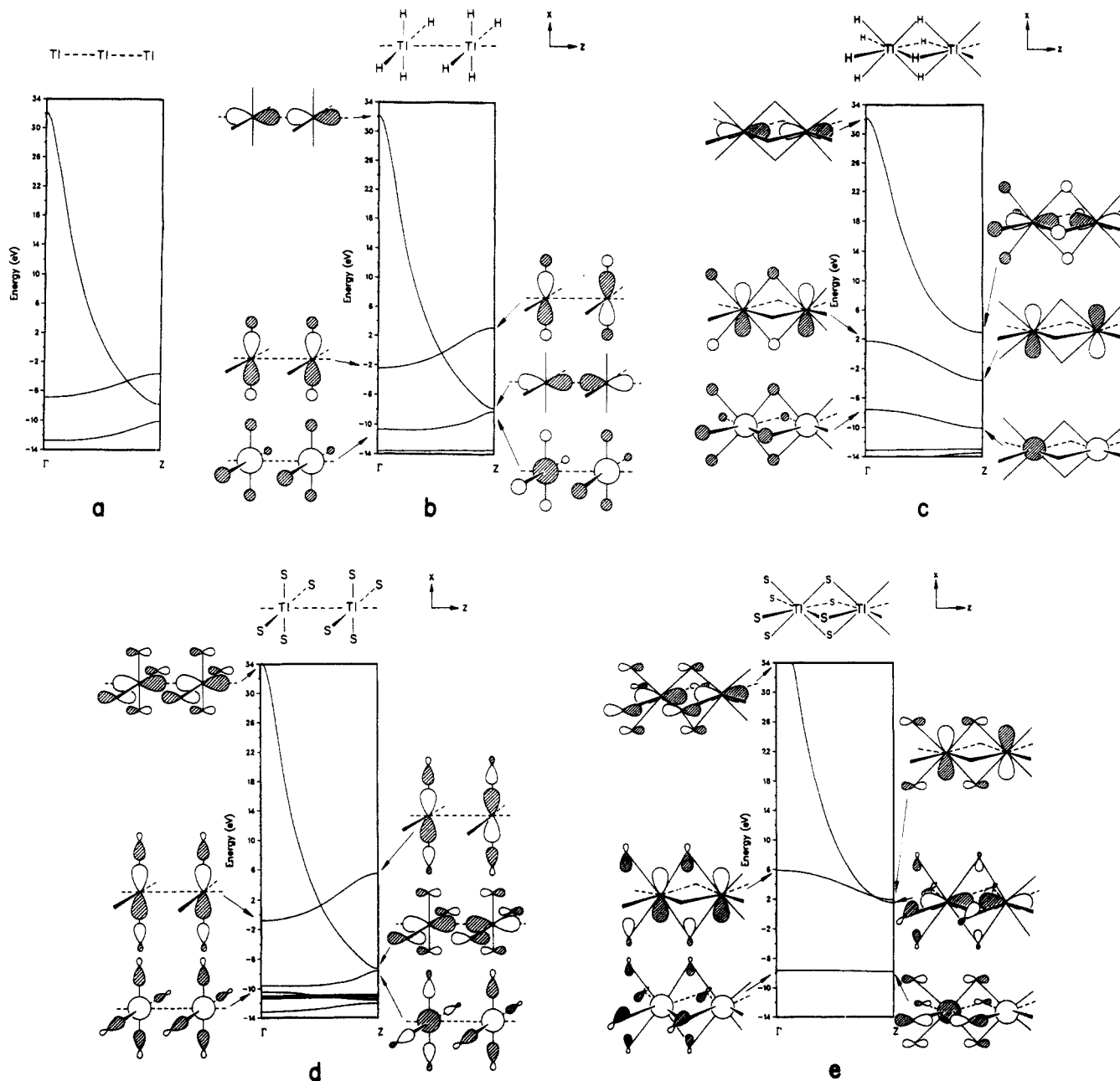


Figure 18. Band structure diagram for Tl chains with different ligand fields: (b) hydrogen square planar, (c) hydrogen cubic, (d) sulfur square planar, and (e) sulfur cubic, with one TlL₄ moiety per unit cell and schematic orbital representations for the Tl bands at Γ and Z to illustrate the different ligand field interactions (only one combination for the degenerate π set, x/y, is shown; ligand bands in b-d are not assigned, and only Tl bands are plotted in e). The band structure for the unligated Tl chain is repeated in a for comparison. Tl-Tl = 370 pm, Tl-H = 267 pm, Tl-S = 324 pm.

simultaneously decreases the amount of s-z mixing, which is important for the Tl...Tl overlap population. This effect is most pronounced in the TlH₄ model chain and can be followed from the DOS projections of the s and z band in Figure 19, where the shaded projections and their integrations indicate the negligible s-z mixing. Again, we point to the direct analogy of eliminated s-z mixing in the cubic field of the Tl₂ dimer.

The, at first, apparently large overlap population for the Tl chain in its realistic three-dimensional square-antiprismatic environment in TlS = Tl^ITl^{III}S₂⁶¹ (Figure 15) has to be seen in light of the longer Tl-S distance of 332 pm vs 324 pm in the model chain. It also should be contrasted with the Tl...Tl overlap population at a 340-pm separation. Also, the Tl^{III} atoms that are covalently bound to S will lower the effective ionic charge on S, thereby decreasing the ligand field strength. The last point may be important, as can be seen from a comparison to a model thallium chain in a square-antiprismatic field with the same geometrical parameters for Tl-Tl (=340 pm) and Tl-S (=332 pm) distances, but without Tl^{III} bound to S (Table VIII). The band structure

of TlTlS₂ from Γ to Z in Figure 20b reveals that the top of the s and the bottom of the z band are even closer than in the band structure of the model thallium chain in a square-antiprismatic field (see Figure 20a; two Tl per unit cell). From a comparison of the band structures in Figure 20 we judge that otherwise the one-dimensional chains, as they were set up, are good models, since the overall shape and splitting pattern of the bands is quite similar. The observed doubling of each band in the full lattice diagram is due to the existence of two Tl^I chains (or 4 Tl^I atoms) in the unit cell. An increased band width or splitting, especially prominent for the x/y band, can be traced to the small interactions with the neighboring parallel chains (550 pm apart) in the other two directions (see Figure 15).

On the other hand, a square-planar ligand arrangement pushes the s-z bands closer together, thus increasing their mixing. The smaller energy separation between the s and z band is apparent from comparing the band structures in Figure 18a,b,d (still no avoided crossing took place at this Tl...Tl separation). The s and z projections in the DOS plots in Figure 21 for the TlH₄ model

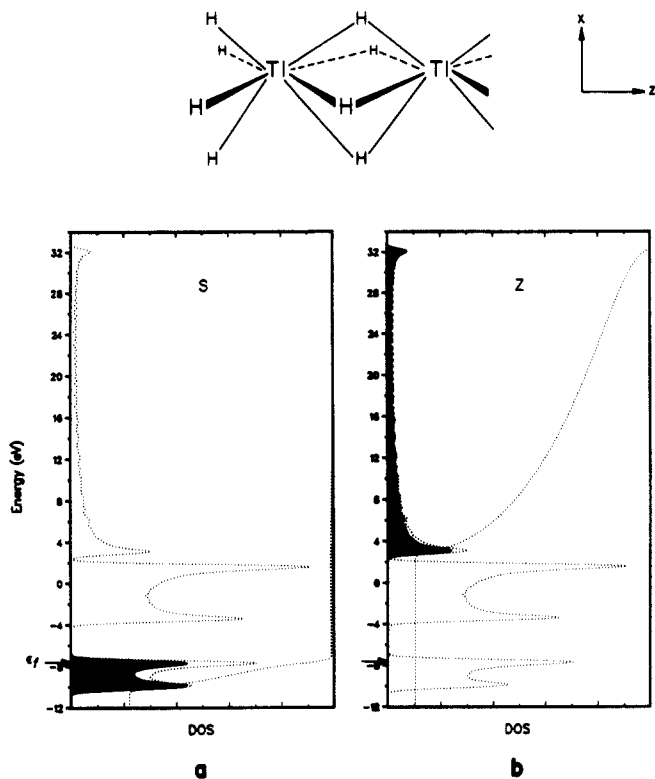


Figure 19. Density of state (DOS) projections for the *s* (a) and *z* (b) orbitals (shaded area) in a linear TIH_4 chain (cubic ligand field) with integrations and total DOS (dotted lines). The Fermi level indication is for $[\text{TIH}_4^{3+}]_n$: $\text{TI-TI} = 370$ pm, $\text{TI-H} = 267$ pm. (Note: The energy window extends down to -12 eV only to exclude the strong hydrogen peak for magnification of the plotted DOS.)

chain with a square-planar ligand arrangement also demonstrate strong *s-z* mixing. The effect is about 20% according to the integrations—up from 12% for the unligated TI chain (compare to DOS projections in Figure 17).

An increased overlap population will lead to shorter metal-metal separations. This could explain in part the extremely short In-In distances of 286 pm found in the linear chains in InMo_4O_6 ,⁷⁵ apparently the only compound so far with a square-planar ligand environment around the chains. The *s* and *z* projections in the DOS plots in Figure 22 for a square-planar InO_4 chain, modeling the InMo_4O_6 system, illustrate the very strong *s-z* mixing (about 40% into each other). From the total DOS outlined in Figure 22, however, it is apparent that a large band gap (of ca. 8 eV) opens up at the Fermi level. This seems at first contradictory to what has just been said, and to what we saw in the band structure diagrams and DOS plots for the square-planar geometry in the TI chains (with $\text{TI-TI} = 370$ pm, Figures 18b,d and 21). However, in the InO_4^{7-} chains an avoided crossing of the *s* and *z* band accompanies the strong mixing. Thus, the actual lines in the diagram are pushed apart from each other.

While our calculations confirm that In-In bonding is important in these chains, we think the high conductivity reported for InMo_4O_6 is unlikely to arise from conduction within the unperturbed In subchain.⁷⁵ The parallel, linear $\text{Mo}_4\text{O}_6^{7-}$ chains, built up from edge sharing Mo octahedra, probably have to account for the conductivity.

However, in the case of InGaSe_2 , which also was found to be conductive along the In chain direction,⁶⁴ the conductivity can probably be attributed to the In chain. Although the exact ligand arrangement for the indiums is not known due to an incommensurate nature of the indium and parallel GaSe_2^- chains, indium seems to have more like a square antiprismatic rather than square-planar environment. In case of a cubic or square-antiprismatic coordination and the existence of an *s-z* avoided crossing, the ligand effect of decreasing the *s-z* interaction will lead to a less pronounced avoided crossing or a smaller band gap. Modeling the InGaSe_2 structure⁶⁴ by a one-dimensional InSe_4^{7-} chain with

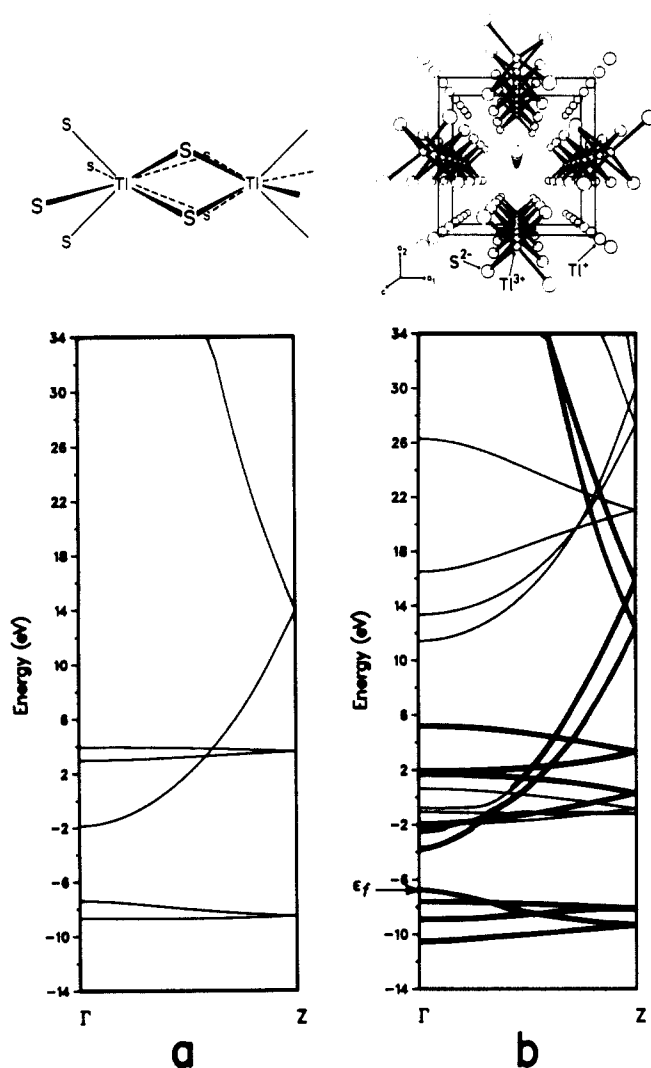


Figure 20. (a) Band structure diagram for a thallium chain in a square antiprismatic ligand field; 2 TI^{I} per unit cell ($\text{TI-TI} = 340$ pm, $\text{TI-S} = 330$ pm). (b) Partial band structure diagram for $\text{TI}^{\text{I}}\text{TI}^{\text{III}}\text{S}_2$ (full, 3-dimensional structure) with only TI^{I} (bold) and TI^{III} bands shown. Doubling of bands with respect to part a due to four formula units (or 2×2 TI^{I}) per unit cell ($\text{TI-TI} = 340$ pm, $\text{TI}^{\text{I}}\text{-S} = 330$ pm, $\text{TI}^{\text{III}}\text{-S} = 260$ pm).

the seleniums in cubic coordination ($\text{In-In} = 315.8$ pm, $\text{In-Se} = 340$ pm) gave a band gap of 0.13 eV.

The similarities and differences in the ligand effects in case of an un/avoided crossing depending on the two different coordination geometries are summarized schematically in Figure 23.

In concluding this section, we once again point to the In_3 and In_6 chain segments in $\text{In}_{11}\text{Mo}_{40}\text{O}_{62}$.⁵⁷ This substructure is a nice example of having both (almost) planarly coordinated and bridged indiums, although they cannot all be considered as In^{I} . While the middle indiums (In^+) within a chain segment have an almost planar oxygen environment ($\text{In-O} = 222\text{--}269$ pm), and very short metal-metal distances (262–267 pm), the top-to-bottom contact between the In^{3+} of neighboring chain segments is 333 pm and bridged by two oxygens.

Square-Planar Thallium Nets. Symmetrical two-dimensional TI arrangements of this kind are found in the ThCr_2Si_2 -type structures $\text{TIM}_2\text{S}_2/\text{Se}_2$ ($\text{M} = \text{Fe}, \text{Co}, \text{Ni}, \text{or Cu}$)^{76–78} (see Figure 24), in $\text{TiCu}_4\text{S}_3/\text{Se}_3$,^{78,79} and in the thallium-containing high- T_c superconductors,^{80–85} for example. For the ThCr_2Si_2 -type structures, the TI-TI distances lie in the range of 374–380 pm with sulfur anions and 385–389 pm with the selenium counterions.

Our way of analyzing the interactions in these TI nets will be the same as was set up in the preceding discussion of the linear chains: start with the bare TI structure and then bring in the ligands at different modes of coordination. A general approach to an analysis of the common structural motif of square nets of

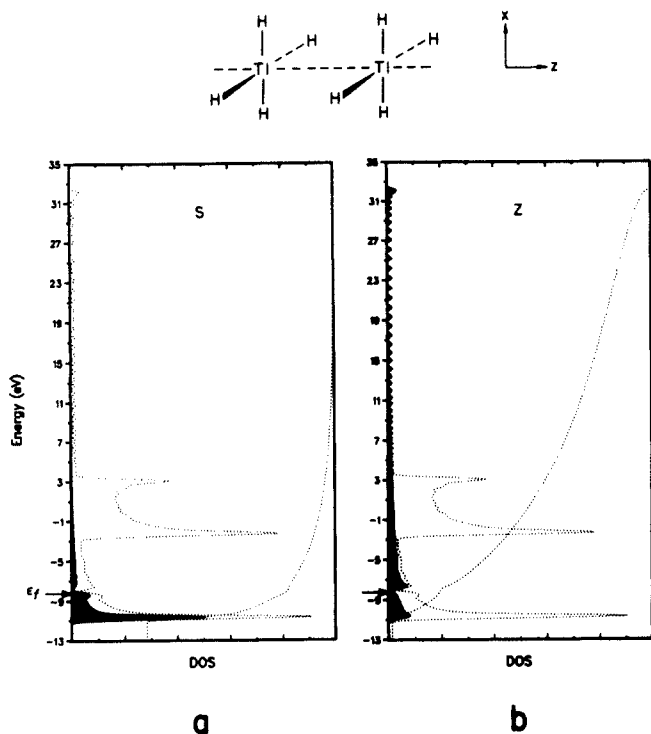


Figure 21. Density of state (DOS) projections for the s (a) and z (b) orbitals (shaded area) in a linear TIH₄ chain (square planar ligand field) with integrations and total DOS (dotted lines). Fermi level for {TIH₄⁺}: TI-TI = 370 pm, TI-H = 267 pm.

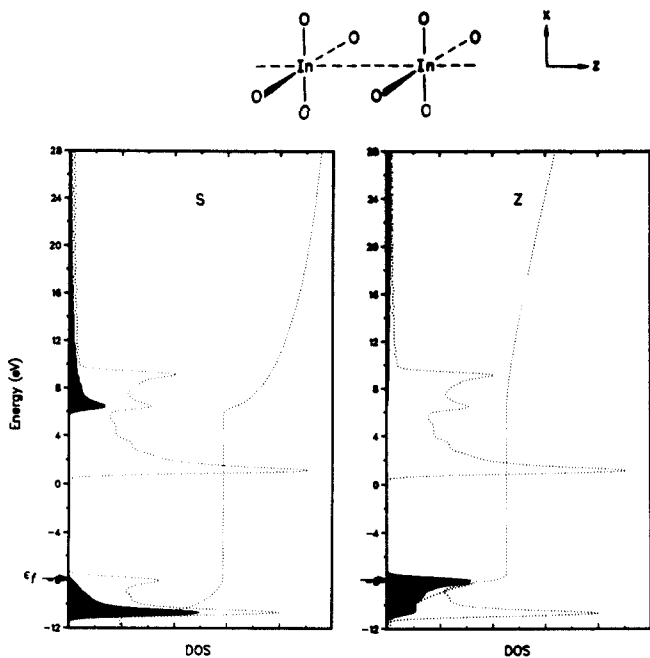


Figure 22. Density of state (DOS) projections for the s (a) and z (b) orbitals (shaded area) in a linear InO₄ chain (square planar ligand field) with integrations and total DOS (dotted lines). Fermi level for {InO₄⁷⁻}: In-In = 290 pm, In-H = 240 pm.

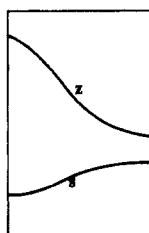
main group elements in solid-state materials was undertaken by Tremel and Hoffmann.¹³¹

While we kept so far a Tl-Tl distance of 370 pm as our point of reference, we now decided to take 390 pm for the nets, in order to keep a reasonable energy window and band width in the diagrams. Due to additional interactions along the second dimension, the bands for the net will be spread out more than the corresponding bands in the one-dimensional chain at the same Tl-Tl distance.

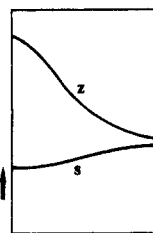
(131) Tremel, W.; Hoffmann, R. *J. Am. Chem. Soc.* 1987, 109, 124.

no avoided crossing

unligated Tl/In chain

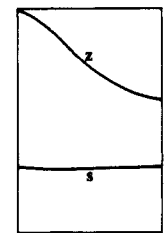


square planar ligand field



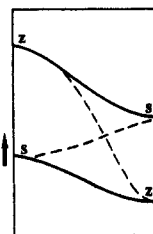
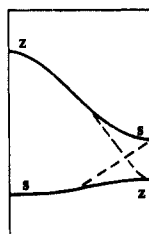
- smaller band gap

cubic or square anti-prismatic ligand field

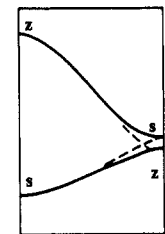


- larger band gap

avoided crossing



- larger band gap



- smaller band gap

in both cases:

- s band pushed up
- stronger s-z mixing
- larger M-M overlap population
- z band pushed up
- weaker s-z mixing
- smaller M-M overlap population

Figure 23. Summaries of ligand field effects on metal chains in cases of an un/avoided crossing, depending on the coordination geometry. Arrows indicate the most important band changes with respect to the unligated metal chain.

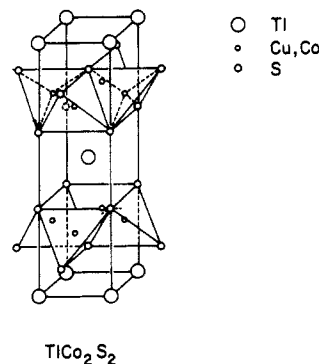


Figure 24. View of the ThCr₂Si₂ structural type with TiCo₂S₂ as an example.

The band structure diagram for a planar square thallium net (lying in the xz plane, with a Tl-Tl separation of 390 pm) is given in Figure 25a, together with a schematic orbital representation at the high-symmetry points. Going along $\Gamma \rightarrow Z$ is equivalent to $\Gamma \rightarrow X$ in a square net, except for the change in character of z and x bands. The symmetry line $Z \rightarrow M$ corresponds to a phase change along the x direction starting at the Z point, and $M \rightarrow \Gamma$ describes a simultaneous phase change in both x and z directions. The symmetry properties of each band are such that along $\Gamma \rightarrow Z$ the z and s bands mix, while from $Z \rightarrow M$ x and s interact. Finally, from $M \rightarrow \Gamma$ both x and z can mix with s as well as with each other. The band formed from the y orbital which is perpendicular to the plane of the net is by symmetry not able to interact with any of the others (just like the x/y band in the one-dimensional chain). At Γ both z and x are degenerate. From Γ to Z the x band runs up, because it goes from σ -antibonding (along x)/ π -bonding (along z) to an all antibonding combination at Z. The reverse is observed for the z band—running down from Γ to Z and reaching an all-bonding combination at M, with additional s mixing in between. The reader is referred to a recent

Table IX. Tl...Tl Overlap Populations for Different Ligand Fields in Two-Dimensional Square-Planar Nets^a

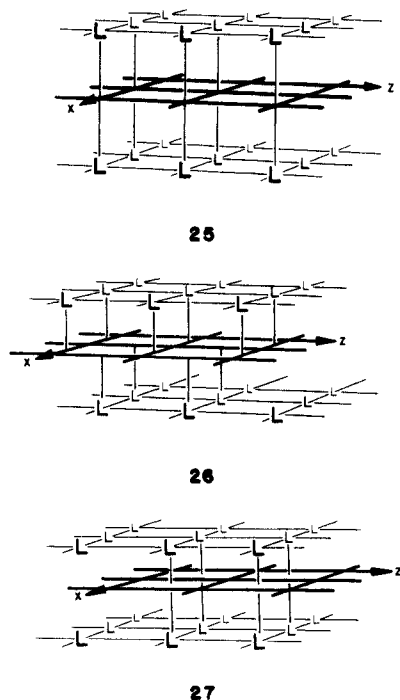
ligand field	L	distance, ppm		overlap pop Tl...Tl
		Tl...Tl	Tl...L	
none, unligated net		370		0.224
		390		0.177
25 , on top/bottom	H	390	267	0.197
	S	390	324	0.197
26 , 2-fold bridging	H	390	267	0.139
	S	390	324	0.155
27 , 4-fold bridging	S	390	324	0.030
	S	374	330	0.102
in 3-dimensional environment, TiCo ₂ S ₂ , see Figure 24	S	374	330	0.098

^a 120K point sets used in calculations, except for the full structure of TiCo₂S₂, where 18K points were employed and the crystallographic coordinates⁷⁶ were used as geometrical input parameters.

book for a qualitative discussion of s,p bands in square lattices.¹¹¹ As pointed out for the perfectly linear chains, a completely filled s band and empty x/y/z bands should not give rise to distortions in such a net.

Table IX lists some Tl...Tl overlap populations along the square edges for different distances. These overlap population numbers are expected to be smaller than the overlap populations in a linear chain with the same Tl...Tl distance, because of additional antibonding combinations in the two-dimensional net.

For a 1:2 Tl:ligand ratio one can imagine three basic symmetrical ligand positions with respect to the Tl square net: the on-top site **25** (of course, the layers come in on bottom as well as on top), the 2-fold bridging position **26**, and the 4-fold bridging (hollow) site **27**.



Each ligand layer forms a square net by itself. These ligand layers sandwich the thallium layer in what could be called either an eclipsed (**25**), semi-staggered (**26**), or staggered (**27**) fashion. In **26** one ligand layer is shifted half a unit cell along x and the other one half a unit cell along z with respect to the thallium net; in **27** both layers are translated half a unit cell along the xz diagonal. The Tl-L distance is kept constant in all three cases. Both **26** and **27** can be thought of as bridging geometries (2-fold and 4-fold, respectively). In **26** each Tl...Tl contact is bridged by one ligand and a distorted tetrahedral ligand environment results for each thallium. In **27** each Tl...Tl edge is bridged by four ligands, to give the familiar cubic coordination sphere around each Tl.

In the known structures, only ligand arrangement **27** has been observed. However, in our theoretical approach, we will also consider possibilities **25** and **26**. Again, we use H⁻ and S²⁻ as model ligands, with Tl-H distances fixed at 267 pm and Tl-S at 324 pm as before. In **27** hydrogen did not lend itself toward a bridging geometry under the constraints of the given Tl-H distance, so we just looked at sulfur as a bridging ligand.

The on-top ligand position **25** corresponds to the square-planar ligand arrangement studied for the linear chains. Indeed the same features are observed; with hydrogen as a ligand, the s and y bands from Figure 25a are pushed up in energy, while the z and x bands remain unaltered. This leads to a somewhat stronger s-z or -x mixing and a larger Tl...Tl overlap population (see Table IX). Sulfur, with its additional p orbitals, also affects the energies of the z and x bands to a slight extent. In both cases, however, the Tl band structure with on-top ligands is quite similar to the one shown in Figure 25a for the unligated Tl net, except for the y band that is distinctively pushed up in energy by the ligand field.

Putting the ligands in the bridging position **26** destroys the horizontal mirror plane as a symmetry element along the net. This allows the y orbital to mix with s, x, and z, depending on the symmetry line. The resulting different looking band structure of Figure 25b, however, is mainly due to avoided crossings, because of the lower symmetry. If it was not for the avoided crossings the general pattern of the band structure would still be just the one seen for the unligated net (follow dotted lines in Figure 25b and compare to Figure 25a), with the y and s band being pushed up in energy. Changes to the ligand-free net are much less pronounced than would be anticipated from the study of bridging ligands in one-dimensional chains. After all, the ligated net **26** has just one ligand bridge per Tl...Tl contact, versus four bridging ligands in the chain. Therefore, the change of slope for the s and y bands from Γ to Z and the strong increase in energy for z at Z, as seen in the chain (Figure 18), are not really visible in the band structure of this net. Only a small decrease in s-z mixing and, correspondingly, in Tl...Tl overlap population is expected and found for **26** (Table IX)—unlike the one-dimensional case (Table VIII).

When the ligands sit in the 4-fold hollow site **27** we approximate most closely the bridging situation in the chain. Sandwiching the Tl net between the displaced ligand nets produces a cubic environment for each Tl in the net, and four ligand bridges per Tl...Tl contact. It is here where we expect the largest change associated with bridging ligands. Indeed, the band structure (Figure 25c), with no avoided crossings altering the "natural" morphology of the bands, looks quite different from its predecessors. As anticipated from the related one-dimensional study, the y band changes slope, with the z band pushed above it (compare to the band structure of the S bridged Tl chain in Figure 18e). The large s-z energy separation leads to a smaller interaction and Tl...Tl overlap population (Table IX), which could be referred to as nonbonding. In the fully 3-dimensional TiCo₂S₂ structure the overlap population rises a little bit, due to a decrease in Tl-Tl and an increase in Tl-S distance. With respect to its Tl subunit, the 3-dimensional TiCo₂S₂ structure is already fairly well modeled by the 2-dimensional TiS₂ net with the same distance parameters (Table IX).

Conclusions

Our calculations show that at long separations it is not so much the Tl...Tl or In...In distance that is important for bonding interactions in molecular and solid-state Tl and In complexes. Within a certain range, a reasonable distance merely provides the potentiality for bonding. If, and to what extent, bonding will occur is largely determined by the ligand geometry. A bridging ligand geometry, be it in a molecular compound or in an extended structure, generally shifts the Tl-Tl/In-In overlap population toward non- or antibonding, when compared to the unligated metal core. In most cases Tl and In units with bridging ligands can be considered as metal-metal nonbonding. On the other hand, an appropriate ligand environment can actually improve the overlap population, respectively bonding interaction, from that seen in the

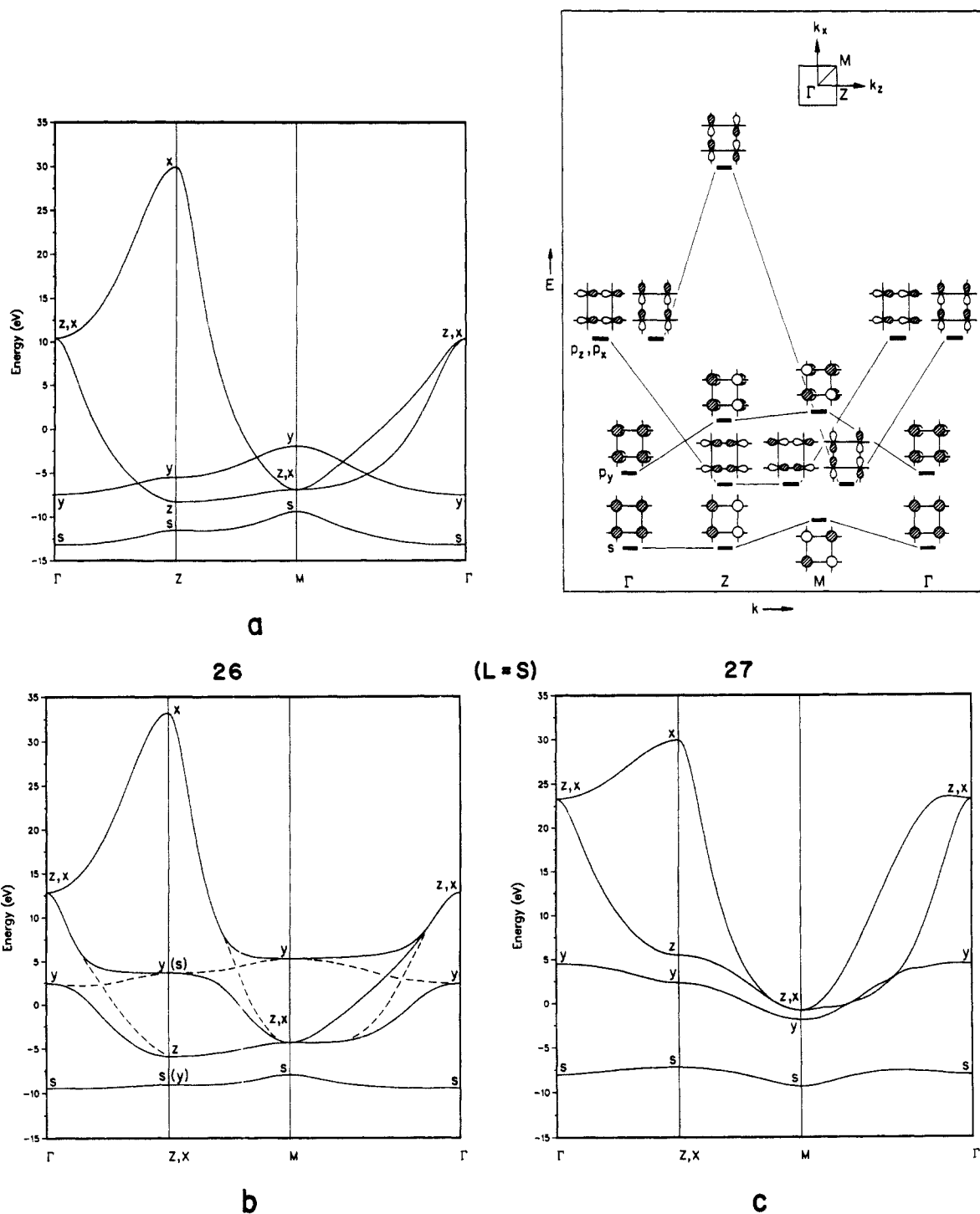


Figure 25. Band structures of square planar thallium nets (Tl-Tl = 390 pm): (a) unligated Tl net, (b) with 2-fold bridging (**26**), and (c) with 4-fold bridging (**27**) sulfur ligands (Tl-S = 324 pm). Only Tl bands are shown. A schematic representation for the Tl orbitals in diagram a is given at its right-hand site.

unligated metal substructure. In molecular complexes a bent geometry with a ligand-M-M angle close to 120° gave an optimum overlap population for systems with Tl^I-Tl^I or In^I-In^I dimers. For extended solids, ligand-M-M angles of 90° (a square planar ligand field for metal chains or an on-top/bottom position in metal nets) gave the optimum overlap population.

However, we still think of most of these optimum metal-metal overlap populations as rather weak bonding interactions, whose significance in structural terms is hard to come by. Concerning the petabenzylcyclopentadienylthallium dimer (**3**, **4**), the molecule that provided the impetus to our work, we feel confident speaking of a Tl^I-Tl^I bonding interaction. But even in this case the geared stacking of the phenyl groups may be important in holding the monomeric units together. Maybe one could agree on the idea that ligand-ligand interactions or packing effects provide for the

general structural arrangement in digging the "big hole" on the potential surface, but that M^I-M^I bonding can be responsible for an additional energy lowering or deepening at the bottom or even in a shift in the equilibrium geometry. This is sketched in **28**.

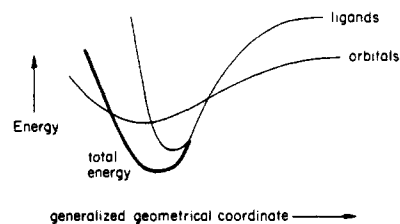
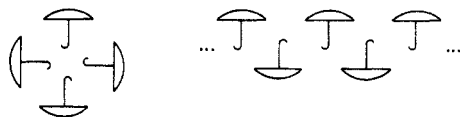


Table X. Parameters Used in the Extended Hückel Calculations

atom	orbital	H_{ii} , eV	ζ_1^a	ζ_2^a	c_1^b	c_2^b	ref
Tl	6s	-11.60	2.30				139
	6p	-5.80	1.60				
In	5s	-12.60	1.903				129
	5p	-6.19	1.677				
C	2s	-21.4	1.625				109
	2p	-11.4	1.625				
H	1s	-13.6	1.3				109
	2s	-32.3	2.275				
O	2p	-14.8	2.275				109
	3s	-20.0	2.122				
S	3p	-11.0	1.827				140
	4s	-20.5	2.44				
Se	4p	-14.4	2.07				141
	5s	-20.8	2.51				
Te	5p	-13.2	2.16				142
	2s	-26.0	1.950				
N	2p	-13.4	1.950				109
	4s	-22.07	2.588				
Br	4p	-13.10	2.131				143
	4s	-9.21	2.0				
Co	4p	-5.29	2.0				127
	3d	-13.18	5.55	2.10	0.5680	0.6060	

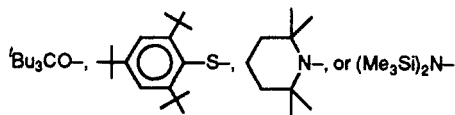
^aSlater exponents. ^bCoefficients used in the double- ζ expansion of the d orbitals.

The packing effects may be illustrated by "umbrella arrangements", shown in **29**. In certain packings of umbrellas¹³² the handles (metals) point toward each other upon optimizing the repulsion (or is it a van der Waals attraction?) among the canopies (bulky ligands).

**29**

Due to the limited number of examples, in both the molecular and solid state, of cases with a close to optimum ligand arrangement and, hence, an increased metal-metal overlap population, further work is needed in finding more structures to develop a better understanding of this fascinating problem.

In the case of molecular complexes, experiments could be aimed at the synthesis of additional examples with nonbridged metal-metal contacts by using bulky ligands without readily available lone pairs, so as to avoid the formation of bridged species. Appropriate ligands may include bulky alkyls or aryls, e.g. the Lappert ligand $(\text{Me}_3\text{Si})_2\text{CH}$ or its analogue $(\text{Me}_3\text{Si})_3\text{C}$. We note a report in the literature on the attempted preparation of $[(\text{Me}_3\text{Si})_2\text{CHIn}]$.¹³³ Also, one might employ oxide, sulfide, or amide ligands, where the lone-pair carrying atom is sufficiently shielded by bulky alkyl substituents. Examples are



(132) The "umbrella picture" was advanced by H. G. von Schnering, MPI für Festkörperforschung, Stuttgart, West Germany, to explain the metal-metal contacts without having to invoke M-M bonding interactions.

(133) Carty, A. J.; Gynane, M. J. S.; Lappert, M. F.; Miles, S. J.; Singh, A.; Taylor, N. J. *Inorg. Chem.* **1980**, *19*, 3637.

complexes with divalent germanium and tin complexes with these ligands were found to be monomeric,^{40a,b,134} but with the larger indium or thallium metal aggregation of the metal centers might occur. We note, however, that the bulky hydridotris(3-*tert*-butyl-1-pyrazolyl)borato ligand $[(\text{HB}(\text{pz})_3, \text{pz} = \text{substituted pyrazol})]$ affords a monomeric Tl(I) complex.¹³⁵

Note Added in Proof: The reader's attention is directed to a recent paper (Budzelaar, P. H. M.; Boersma, J. *Recl. Trav. Chim. Pays-Bas*, **1990**, *109*, 187) for a theoretical discussion of the bonding in In and Tl cyclopentadienyls.

Appendix

The computations were performed within the extended Hückel formalism,^{109,136} with weighted H_{ij} 's.¹³⁷ The atomic parameters for the elements involved in our calculations are given in Table X. Geometrical parameters and K-point sets are referred to in appropriate Tables (see footnotes) or in the text. The K-point sets for the average property (overlap population) calculations in the two- and three-dimensional cases were chosen according to the literature.¹³⁸ Our attempts to trace down a maybe more widely checked set of thallium parameters were unsuccessful. Calculations on thallium molybdenum systems, TlMo_3Se_3 , unfortunately do not report any Tl parameters:^{112,144,145} Reference 146 gives the following optimized orbital exponents for neutral Tl in its ground state: 6s 2.1366; 6p 2.0423. Different sets of H_{ii} values can be found in refs 147 and 148.

Acknowledgment. We thank the Deutscher Akademischer Austauschdienst (DAAD) for the award of a NATO postdoctoral fellowship for C.J. and the National Science Foundation for its generous support through Grant CHE-89 12070. We are grateful to Jane Jorgensen and Elisabeth Fields for their expert drawings.

(134) (a) Lappert, M. F.; Slade, M. J.; Atwood, J. L.; Zaworotko, M. J. *J. Chem. Soc., Chem. Commun.* **1980**, 621. (b) Fjeldberg, T.; Hope, H.; Lappert, M. F.; Power, P. P.; Thorne, A. J. *J. Chem. Soc., Chem. Commun.* **1983**, 639.

(135) Cowley, A. H.; Geerts, R. L.; Nunn, C. M.; Trofimenko, S. J. *Organomet. Chem.* **1989**, *365*, 19.

(136) (a) Hoffmann, R.; Lipscomb, W. N. *J. Chem. Phys.* **1962**, *36*, 2179; **1962**, *37*, 2872. (b) Whangbo, M.-H.; Hoffmann, R.; Woodward, R. B. *Proc. R. Soc. London, Ser. A* **1979**, *366*, 23.

(137) Ammeter, J. H.; Bürgi, H.-B.; Thibeault, J. C.; Hoffmann, R. *J. Am. Chem. Soc.* **1978**, *100*, 3686.

(138) (a) Ramirez, R.; Böhm, M. C. *Int. J. Quantum. Chem.* **1986**, *30*, 391. (b) *Ibid.* **1988**, *34*, 571.

(139) Albright, T. A. Personal communication, 1988.

(140) Chen, M. M. L.; Hoffmann, R. *J. Am. Chem. Soc.* **1976**, *98*, 1647.

(141) Hoffmann, R.; Shaik, S.; Scott, J. C.; Whangbo, M.-H.; Foshee, M. *J. Solid State Chem.* **1980**, *34*, 263.

(142) Canadell, E.; Mathey, Y.; Whangbo, M.-H. *J. Am. Chem. Soc.* **1988**, *110*, 104.

(143) Hinze, J.; Jaffé, H. H. *J. Phys. Chem.* **1963**, *67*, 1501.

(144) (a) Hughbanks, T.; Hoffmann, R. *J. Am. Chem. Soc.* **1983**, *105*, 1150. (b) Hughbanks, T.; Hoffmann, R. *Inorg. Chem.* **1982**, *21*, 3578.

(145) Kelly, P. J.; Anderson, O. T. In *Superconductivity in d-, f-Band Metals*; Proceedings of the 4th Conference; Buckel, W., Weber, W., Eds.; 1982; pp 137-140.

(146) Clementi, E.; Raimondi, D. L.; Reinhardt, W. P. *J. Chem. Phys.* **1967**, *47*, 1300.

(147) Desclaux, J. P. *At. Data Nucl. Data Tables* **1973**, *12*, 311.

(148) Herman, F.; Skillman, S. In *Atomic Structure Calculations*; Prentice-Hall, Englewood Cliffs, NJ, 1963.